Feature specific neuronal oscillations in cortical layers

T. Clausner, J. Marques, R. Scheeringa, M. Bonnefond

Feature specific neuronal oscillations in cortical layers

Clausner, T.[1,2], Marques, J.[2], & Scheeringa, R.[1,2*], Bonnefond, M.[1*]

31st July 2024

* both authors contributed equally to the project

[1] Lyon Neuroscience Research Center, Computation, Cognition and Neurophysiology (Cophy) team, INSERM UMRS 1028, CNRS UMR 5292, Université Claude Bernard Lyon 1, France

[2] Donders Institute for Brain Cognition and Behaviour, Radboud University, NL-6500 HB Nijmegen, The Netherlands

Abstract

The particular role of cortical oscillations has been a long-debated topic that resulted in a variety of theoretical frameworks. Oscillatory activity in the α band has been associated with sensory processing, attention as well as other cognitive functions, while γ band oscillations is thought to be related to stimulus feature processing. Current theoretical frameworks rely on the separation of the cortical architecture into layers. Recently, methodological advancements have allowed to test layer specific frameworks on the role of oscillations in cortical computations in healthy human participants. Using EEG-fMRI, we have investigated for the first time both, stimulus feature specificity (line orientation) and the relationship between the laminar BOLD activity and α and γ band oscillations. We find γ oscillations to be positively correlated with feature-specific signals in superficial layers as predicted by the literature, but we found a deep layer contribution as well. Furthermore we found a layer (and frequency) dissociation within the α band for general, feature unspecific, processes and a feature related process. The power of the α-band correlated negatively with feature unspecific neural activity in all cortical layers. We further found that high frequency α oscillations were specifically related to stimulus feature specific BOLD signal in deep and superficial layers. More interestingly, we also observed a general modulation effect for negative BOLD signal deflections in line with the inhibitory role of α during visual attention in superficial layers. Those findings support the association of γ band oscillations with visual feature processing and further point towards the involvement of multiple α oscillations in more general and feature related processes.

Keywords: laminar, fMRI, EEG, alpha, gamma, oscillations, visual features

Introduction

The involvement of brain oscillations in cortical computations and their role in laminar communication channels are highly debated in the scientific community. Although the significance of γ band oscillations for cortical computations remains uncertain [1–4], they have been associated with bottom up stimulus feature specific processing [5, 6]. In line with anatomical findings, γ band oscillations are primarily associated with neuronal activity in granular and supragranular layers [7]. Hence, nearly all current frameworks predict that γ band oscillations should be observed specifically during ongoing stimulus feature processing in supra-granular layers [6–8].

In contrast, low-frequency oscillations (α oscillations, particularly) were commonly thought to reflect a general inhibitory process [9, 10]. However, recent empirical evidence [11–13] and theoretical work [8, 14, 15] suggest that α might play a much more differential role in cortical information processing and routing. Evidence suggests that α oscillations are expressed in all cortical layers, although the debate regarding their laminar profile in the cortex is still ongoing [16–18]. Discrepancies have led to the assumption that α band activity reflects a family of low-frequency oscillations that serve functionally distinct roles and act more specifically than previously anticipated [8, 19]. A common finding is that α oscillations are mainly linked to feedback-directed activity, implying the involvement of top-down processes [16], possibly coordinated with the involvement of the pulvinar [20] (but see Lozano & VanRullen 2019 [21]).

The framework proposed by Bonnefond et al. (2017) [8] posits that α oscillations are involved in establishing task- or stimulus-specific communication channels in the feedback direction by synchronizing low-power α band activity in source and target regions (see also Harvey et al., 2013 [22] and van Kerkoerle et al., 2014 [16]). This suggests that α band oscil-

lations are tightly linked to the activity of neuronal populations processing specific stimulus features, or at least receptive fields, which contradicts the prevailing idea of low spatial selectivity of α. Additionally, the framework predicts that the communication channel is established in supra-granular layers, as described in the original publication. The framework emphasizes that the actual communication is established via source-target α band coherence, while the selection of neurons (e.g., through attention-related processes) is related to α power changes (i.e., low α power in relevant and high α power in irrelevant pools of neurons). These two processes may be dissociated through distinct laminar activation profiles. Stimulus-induced γ oscillations or spiking activity [23] might be locally controlled by these α oscillations, which are nested within the excitable phase of α, and then transferred to the next hierarchical level for further processing.

Testing the proposed framework necessitates a thorough investigation of feature specific cortical activity on the laminar level, which has traditionally posed a challenge in healthy human participants. Hence, most evidence has been obtained from animal models. Past studies have primarily focused on methodological obstacles [18, 24, 25] or have relied on laminar level functional magnetic resonance imaging (fMRI) alone [26–30]. However, fMRI lacks temporal resolution and serves as a proxy for neuronal activity. In contrast, electroencephalography (EEG) and magnetoencphalography (MEG) directly record neuronal activity, but have relatively low spatial resolution due to the mixture of different signals they record. Recent studies combining high-resolution (laminar-level) fMRI with EEG recordings have successfully addressed these limitations [18, 31]. In our study, we employed this approach to investigate, for the first time, feature-specific BOLD signals in the deep (infra-granular), middle (granular), and superficial (supra-granular) cortical layers in primary visual regions. The proposed framework emphasizes the role of α oscillations in selecting pools of neurons relevant to the task and inhibiting potentially interfering or unwanted information. Therefore, we not only examined the relationship between EEG and positive BOLD signal deflections but also related EEG power changes to negative BOLD deflections, which has received less attention and mostly focused on the default mode network [32–34]. However, sparse evidence suggests that negative BOLD deflections contribute to understanding ongoing neuronal processing and specifically the inhibition of unwanted information [35, 36]. In our analyses, we focused on feature-specific and feature-unspecific BOLD signal changes (including negative deflections), highlighting the general importance of studying BOLD signal decreases for functional tasks.

The primary aim of this study was to investigate the relationship between cortical oscillations and feature-specific and feature-unspecific BOLD signals across multiple cortical layers. For this we used a visual oddball task where only the standard stimuli consisting of two orthogonal stimulus gratings offset by 90° were our features of interest. Our results demonstrate that γ band activity not only relates to the feature-specific superficial layer BOLD signal [8, 16, 18, 37] but also to deep layer BOLD activity. Additionally, we found that general modulatory, feature unspecific processes, potentially associated with attention related mechanisms, and feature-specific laminar activation profiles were linked to distinct α frequency bands.

This study provides the first direct evidence in healthy human participants that low-frequency oscillations serve multiple purposes in the visual cortex, associated with distinct cortical layer profiles.

Methods and Materials

Participants

A dataset consisting of 52 right-handed individuals (34 of whom identified as female) between the ages of 18 and 35 ($\mu = 24.0$, $\sigma = 4.0$) was collected. We only included participants who did not need eye correction (due to practical reason concerning the scanning procedure) and did not have a history of neurological or psychiatric issues or had not undergone neurosurgery. All participants provided informed consent and were monetarily rewarded for their participation. The study received ethical approval from the local ethics committee.

Data Acquisition

Functional and anatomical magnetic resonance imaging (fMRI) data was collected using a Siemens MAGNETOM Prismafit 3T MRI scanner equipped with a 64-channel whole head and neck coil. Before entering the scanner, each subject received detailed instructions and was given the opportunity to practice the main experiment in a short block. Once prepared, the subject was placed inside the scanner. A T1-weighted scan was acquired in the saggital orientation using a 3D MPRAGE sequence [38] with the following parameters : $TR/TI = 2.2/1.1s$, 11° flip angle, FOV 256 × 256 × 180 mm and a 0.8 mm isotropic resolution. Parallel imaging($iPAT = 2$) was used to accelerate the acquisition resulting in an acquisition time of 6 min and 31 s. For the functional data, we utilized a 3D gradient-EPI [39] with CAIPI acceleration capabilities [40] as implemented by Stirnberg et al. [41]. A partial brain acquisition using a coronal slab was encoded with a FOV $208.8 \times 208.8 \times 39.6$ mm covering most occipital and parietal lobes, incluing primary visual regions. The flip angle was set to 20°, resulting in a near isotropic voxel size of $0.9052 \times 0.9052 \times 0.9$ mm (volume TR: 3.3 s; TE: 34 ms). The sequence was modified to allow an arbitrary time delay between every 3 consecutive volumes. Here, the delay was set to 3 s to ensure unperturbed EEG data acquisition during this delay and that the whole BOLD HRF could be subsequently sampled afterwards.

This protocol was used for both, the main experiment and the retinotopic field mapping. However, for the latter the sequence gap was omitted because no EEG data was recorded. Each experimental block started with six dummy volumes to allow for the magnetization to reach a steady state, but only the last three of those dummy volumes were actually recorded (and later removed for the data analysis).

In addition, we simultaneously recorded EEG data using a 64 channel MR compatible EEG system [42] at a sampling rate of $5k$ Hz. Impedances were kept below $20k$ Ω during subject preparation. Electrode positions were recorded using a photogrammetry-based approach, as described in Clausner et al. (2017) [43]. A 3D model, computed from approximately 50 photographs of participants wearing an EEG cap, was aligned via facial features to a 3D representation of the anatomical MRI. Electrode positions were determined from the photogrammetry based 3D model, transformed into MRI

space and projected along the vertex normals to the MRI scalp surface.

Furthermore, eye-tracking data was simultaneously collected using an EyeLink 1000+ [44], but later omitted from the analysis protocol due to insufficient data quality and cumbersome handling in the scanner.

The full experimental protocol comprised a high-resolution anatomical T1 scan lasting for 8 min, followed by four consecutive blocks of EEG-fMRI recordings for the main experiment. Each block lasted for 14 min, with a total duration of $4 \times 14 = 56$ min. Three blocks of population receptive field (pRF) mapping were recorded hereafter, each block lasting for 7 min, utilizing the same fMRI recording sequence but without the 3 s pause for clean EEG data recording ($3 \times 7 = 21$ min). Additionally, 20 resting-state volumes of that sequence with an inverted flip angle lasting 1 min were acquired for distortion field estimation. However, this was not included in the final analysis protocol. Instead a non-linear recursive boundary estimation [45] was used that simultaneously provides the cortical layer estimation (explained in detail below). The total duration of the experiment was approximately 150 min, including ≈ 40 min preparation time, a $5-10$ min break between the two main experimental parts, and 15 min for participants to wash and dry their hair after the experiment.

Stimulus presentation

Stimuli were projected onto a screen behind the subject's head using an EIKI LC XL100 projector (`https://www.eiki.com/`) with a resolution of 1024×768 px and a maximum brightness of 5,000 ANSI-lumen, and a contrast ratio of $1000:1$. The effective field of view comprised a $24 \times 18°$ visual angle at a distance of 855 mm relative to the subject's eyes. Throughout the entire experiment, stimuli were presented in an otherwise dark scanner room. During the anatomical scan, participants were able to read the experiment instructions again and were asked to remain still with their eyes either opened or closed for the rest of the recording.

Main experiment

Participants performed a demanding visual attention task, using central stimulus presentation. The stimuli could either be left (counterclockwise) or right (clockwise) oriented gratings ($\pm 45°$ relative to the vertical axis of the screen). A subtle wavy pattern was incorporated as oddball stimuli and participants were instructed to respond to them using their right index finger. The non-oddball to oddball ratio was set to $5:1$. Stimuli were presented on a gray background with 50% luminance, using the "Presentation" software [46]. A fixation indicator was designed based on the findings of Thaler et al. (2013) [47], which consisted of a black, filled circle overlaid with a white cross (also known as the "Greek cross"), containing a central fixation dot (see Figure 1). This design was found to yield higher fixation performance compared to traditional fixation stimuli, such as simple crosses or dots. In our experiment, the central fixation dot at the centre of the fixation indicator was either red or green, indicating to the participant whether they should avoid blinking (red = avoid blinking).

Feature specific (left or right oriented) stimuli were constructed as Tukey-filtered gratings of 8° visual angle in diameter and a spatial frequency of alternating bright and dark lines of 3.125 cycles per $1° = 25$ cycles that were presented at the central screen location. The contrast between bright and dark components was set to 70% luminance change. An area of 0.8° visual angle in diameter was cut out centrally to house the fixation mark. Gratings could be presented in either left or right orientation, deviating $\pm 45°$ from the vertical axis. Additionally, oddball trials were constructed similarly, but with a slightly wavy pattern of an amplitude of 0.3571° visual angle and a frequency of 0.6526 cycles per degree visual angle ($\approx$ 4 cycles across the diameter of the stimulus area). Furthermore four different phase offsets $\left[0, \frac{\pi}{2}, \pi, \frac{3\pi}{2}\right]$ were used in a pseudo-randomized, counter-balanced manner. The outer edge of the stimulus, as well as the edge towards the inner cut-out where the fixation was placed, was filtered using a Tukey filter, to avoid sharp edges.

All settings concerning stimulus appearance were extensively piloted to obtain a satisfactory trade-off between difficulty and accuracy. An example for an oddball stimulus can be found in Figure 1 A.

Receptive field mapping

To identify visual cortex regions of interest (ROIs), a population receptive field (pRF) mapping was conducted to obtain structural locations of V1, V2, and V3 for both hemispheres [48]. The experiment consisted of three blocks, with 128 volumes recorded for each block. The stimulus presentation was implemented using the VistaDisp software package [49] in PsychToolbox [50]. A sequence of full-contrast checkered bars was presented, moving in different directions (W $\rightarrow$ E, SE $\rightarrow$ NW, N $\rightarrow$ S, and SW $\rightarrow$ NE) and their reverse directions in front of an otherwise empty screen of 50% luminance. The bars were 2.25° visual angle wide and up to 18° visual angle long, filling a circular area of 18° visual angle in diameter. The overlap with neighbouring bar locations was 1.125° (half a bar's width). Sixteen different locations along the directional axis for each moving direction were sampled, resulting in 128 trials per block, with each location being sampled twice. Each location had an alternating full-contrast black and white pattern presented five times for 0.66 s per cycle (= 0.66 s for 2 alternations). One volume was recorded for one of the sets of five consecutive pattern repetition cycles. For each diagonal moving direction, the pattern disappeared for the last eight locations (40 cycles) of that direction to allow for the BOLD response to fall back to baseline. The procedure is further described in Alvarez et al. [51].

Experimental Procedure

The sequence of events that forms a trial, as well as how the interleaved data acquisition sequence was constructed is illustrated in Figure 1 A. After participants were instructed and informed consent was collected, the EEG cap was fitted and electrode positions were recorded. Hereafter electrode housings were filled with an electrically conducting gel to bridge the gap between the electrodes and the skull. Afterwards participants were placed inside the scanner. Foam and pillows helped to keep the participant's head stable and to remain comfortable throughout the experiment. A strap of tape across the forehead provided additional tactile feedback of any head motion and contributed to minimizing head

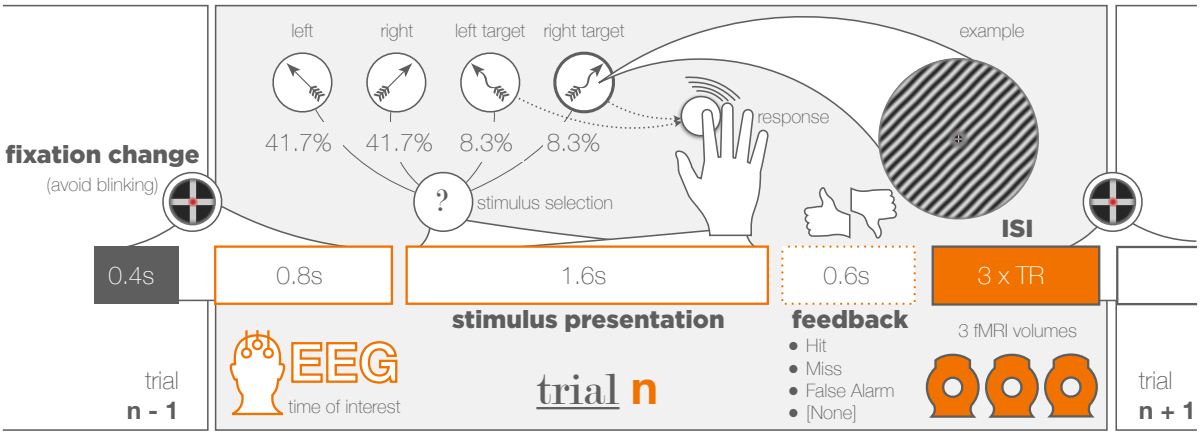

Figure 1: **Experimental Procedure of the main experiment.** 1.2 s prior to the stimulus onset the fixation indicator would turn from green to red, indicating the subject to avoid blinking. After a period of 0.4 s (0.8 s before stimulus onset) the last fMRI volume of the previous trial finished recording. For a period of 3 s no fMRI data is collected in order to avoid gradient artifacts in the EEG data. The stimulus presented is a left or right (±45° from vertical axis) oriented grating. In 16.7% of stimuli (2 × 8.3% for left and right respectively) the linear pattern of the grating would have a slight wiggly pattern (see example grating). Participants were ask to respond to those oddball trials with a button press. If no oddball trial was presented, the stimulus would remain on the screen for 1.6 s, followed by a 0.6 s period where only the fixation indicator is shown. In case of a response, corresponding feedback ("correct", "false alarm" or "miss") is displayed instead. Afterwards, the fixation indicator turns back to green, indicating the subject that the period to avoid blinking has ended. Now, three consecutive 3D EPI volumes (TR : 3.3 s) are recorded, before the next trial starts. Overall, 240 trials (four blocks with 60 trials each) have been collected. Additionally, a high resolution (0.8 mm iso voxel size) T1 weighted full brain image has been collected before the main experiment to obtain individual subject's anatomy. Furthermore, three blocks of pRF mapping (128 trials each) have been performed after the main experiment using the same fMRI sequence as in the main experiment (without gaps).

movements. The eye tracking device was set up and calibrated after that. Before the main experiment started - during the high resolution T1 weighted anatomical scan was - a practice block was performed for the actual task that followed hereafter. The practice block was a slightly modified version of the main task, such that the inter-stimulus-interval (ISI) was shortened and the ratio of oddball over non-oddball trials was increased to 1 : 3 to facilitate the training effect. The main experiment consisted of four blocks of 60 trials each, ten of which were oddball trials that were excluded from the later analysis. Participants were instructed to respond as fast as possible to the occurrence of such a trial by pressing the response button with their right index finger.

A trial was defined as the following sequence of events: 1.2 s *before* the stimulus onset the central dot of the fixation mark would turn red (indicating the subject to avoid blinking). With a probability of $p = 0.167$ an oddball trial would be shown and otherwise a regular stimulus for 1.6 s. If no oddball was shown and the subject did not respond by a button press, the red fixation stayed for additional 0.6 s before turning back to green, which would end the trial. In all other cases the subject would receive feedback in form of a centrally presented text indicating *hit*, *miss* or *false alarm*, followed by the green central fixation. Hence, each trial would in any case last $1.2 + 1.6 + 0.6 = 3.4$ s of which the last 3 s went into the EEG analysis. During the last 3 s before the trial ended, MRI gradients and RF pulses were switched off, such that no MR data could be collected. This was done to ensure good EEG data quality. After each trial, three partial brain 3D EPI volumes ($TR = 3.3$ s) were recorded, sampling the BOLD response for a single stimulus presentation of that length [52].

For each of the four experimental blocks, 60 trials were presented, resulting in 240 trials per participant in total. Since trials could be constructed as left or right oriented gratings and oddball or non-oddball trials, four possible trial types could occur. Since the ratio between non-oddball and oddball trials was fixed at 5 : 1, each block consisted of five oddball and 25 non-oddball trials and therefore in total 20 oddball and 100 non-oddball trials for each orientation respectively ($\sum = 240$). The four different phase-offsets were unevenly distributed within blocks but counterbalanced across the experiment.

After the main experiment, participants could voluntarily rest for some minutes before the population receptive field (pRF) mapping [53] was performed. Central fixation during pRF mapping was ensured by a fixation dot that randomly changed colour between red and green at an average rate of 1 change per 3.3 s. This corresponds to 1 TR, since the same fMRI protocol as for the main experiment has been used, only without the gaps that allow more noise free EEG recordings during the main experiment. Participants were instructed to indicate a colour change by a button press with their right index finger. All three blocks for pRF mapping were recorded consecutively without a break, except for subject $S11$, where only the first two blocks were recorded due to the subject feeling uncomfortable in the scanner.

Data processing

Data analyses were performed using the following software packages and toolboxes: analyzePRF [53, 54], ANTs [55], FieldTrip [56], Freesurfer [57], FSL [58], janus3D [43], Metashape [59], MRICron [60], MRI Volume Masker 3000 TM [61], MrVista [49], OpenFmriAnalysis [45], SPM12 [62] and Workbench [63], including respective dependencies in either Bash, Python or MATLAB. All analysis scripts can be downloaded from: [link will be provided soon].

No participants have been excluded from any of the analyses. For the main experiment, trials were selected for both non-oddball conditions (= 25 trials per orientation per block = 200 trials per subject). Trials were only excluded in case of a false alarm response or if major EEG artifacts such as

significant muscle artifacts during the period of interest have been detected, which was the case in $\approx 2\%$ of all trials.

fMRI Motion Correction and Co-registration

A critical step in laminar fMRI is the correction for motion and co-registration of functional and anatomical data since even sub-millimeter misalignments affect the laminar segmentation substantially. Motion parameter estimation and correction was done using ANTs [55]. As a first step, the first three volumes were removed from each set of volumes (for the three blocks of pRF mapping and the four blocks of the main experiment). Afterwards a manually drawn brain mask was created for every first volume of the first main experiment block and the first pRF mapping block using MRI Volume Masker 3000 TM [61]. Automatically generated masks were manually "fine tuned", such that the outer boundary was enclosing the gray matter as close as possible. Extensive parts of cerebrospinal fluid, fatty components, arteries and other tissue were carefully excluded from the masks. The resulting masks were used to constrain motion parameter estimation and to correct the anatomical segmentation performed by Freesurfer [57] within the respective region of interest (the field of view of the functional scans). The actual motion parameter estimation was then performed in two stages. In the first stage all volumes of one recording block were registered to the within-average over time of that block. During the second stage all newly computed within-block averages were registered to the first volume of the first block of the main experiment. Thus all blocks, including pRF mapping, used the first volume of the first block of the main experiment as the final reference. While for the first stage a rigid body transformation was used, an affine transformation was computed for the second stage. The initial linear transformation in that stage was followed by a non-linear transformation using symmetric normalization (SyN) [64].

A similar approach was used for functional to anatomical partial volume co-registration, including a rigid body, affine and non-linear transformation using symmetric normalization. Note, that the T1 weighted image was registered to the functional data (and not vise versa) to map the laminar segmentation that is obtained from the anatomical T1 (see below) to functional data space. All estimated motion parameters were combined and applied in a single operation to ensure that functional data was interpolated only once [65].

Anatomical Segmentation

In a first step, the manually drawn functional masks were registered to native T1 space. This was done in order to ensure proper anatomical segmentation performed using FreeSurfer [57]. This procedure greatly improved the later non-linear boundary registration of pial and white matter boundaries of functional and anatomical data, which are used for the construction of cortical layers and correct for field distortions. In detail, after the initial full brain segmentation, respective functional brain masks obtained as described above were fit to the full brain mask and replaced the respective parietal parts that were covered by the functional data. Hereafter the estimation of pial and white matter surface boundaries was recomputed. Corrected pial surfaces and uncorrected white matter surfaces were used as boundaries for the later laminar segmentation as this procedure makes use of the surface's boundaries.

Population Receptive Field Mapping

Population receptive field (pRF) mapping was performed as implemented in the open source tool-box analyzePRF. More detailed information about the algorithmic implementation can be found in the reference literature [53, 54]. Binarized versions of each stimulation frame served as spatial regressors for the underlying general linear model (GLM). Each of the presented 64 unique bar locations (including blanks) were thresholded such that the background received a value of 0 and the entire bar irrespective of the checkerboard pattern received a value of 1. In order to save computation time, stimuli were downsampled from screen resolution to a resolution of $192 \times 192\ px$. A Savitzky–Golay filter with a filter window of 61 TR s (201 seconds) was applied to the data. The data then was converted into percent signal change relative to the median. Whereas the Savitzky–Golay filter was applied for each experimental block separately, percent signal change was computed over all blocks combined. Based on a GLM - including third order polynomials - parameters were estimated for orientation (angle), distance to the centre of the screen (eccentricity) and the explained variance per voxel (R^2). The gray matter mask, obtained from the anatomical segmentation, was applied and only gray matter voxel locations were fed into the pRF analysis. Based on those maps, regions of interest (V1-3) were manually labelled using Freeview. To facilitate the manual drawing process, a functional atlas [66] containing all regions of interest was anatomically fitted to the functional data beforehand. Fitted regions from the atlas were overlaid together with the results of the pRF mapping onto the inflated pial surface as obtained from Freesurfer. Marked labels were then transformed into volumetric data and into functional data space using previously computed co-registration transformation matrices and volumes. It should be noted however, that regions V2 and V3 could not be reliably separated in all participants due to poor data quality. Hence, all analyses will focus on V1 only, but results for V2 and V3 are provided within the supplementary material (see Figures Sf1, Sf3 and Sf4 and Tables St2 and Tables St3).

Estimation of Cortical Layers

Laminar segmentation was performed using co-registered gray and white matter boundaries as references for upper and lower bounds of the segmentation. In order to resolve cortical depth precisely, the curvature of the anatomical boundaries was taken into account. This is necessary since the relative thickness of cortical layers varies depending on the cortical curvature [67]. Each voxel covered by the gray matter mask, received a weight as a function of its volume belonging to each of the shell-like meshes forming the boundaries. If a layer boundary would cut the voxel exactly in half, adjacent layers would receive a weight of 0.5 each. Hence, voxels were not separately treated as belonging to different layers, but rather their signal was seen as a weighted mixture coming from different layers. Thus, a voxel located towards the white matter boundary would contribute more to the signal generated in deeper layers - receiving a higher weight - as compared to a voxel being closer to the surface, which would receive a lower weight at the reference location [68]. Layer weights were computed using the open source toolbox OpenFmriAnalysis. As a result, five layer weights per voxel were obtained (CSF, superficial, middle, deep and white matter layer).

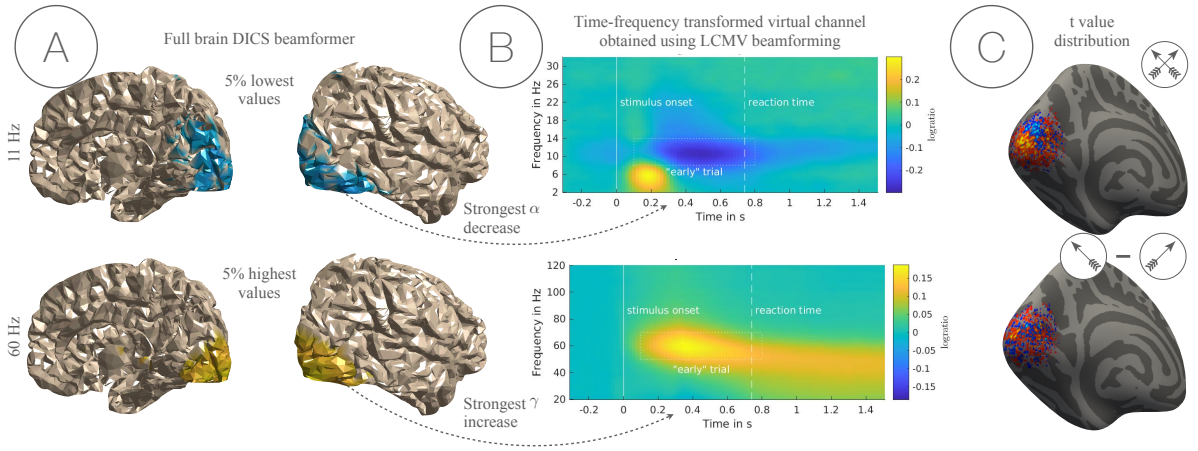

Figure 2: Intermediate results to sanity check the EEG and fMRI data. **A) Full brain DICS beamformer results.** Subject average of log-ratios between stimulus and baseline for 11 Hz (α)and 60 Hz (γ) for both sets of separately filtered EEG data. This serves illustrative purposes only, since the virtual channels of interest have been selected from time-frequency transformed virtual channels obtained using LCMV beamforming. Here the 5% vertices with the strongest decrease (top) or increase (bottom) are shown. **B) Time-frequency representation of virtual EEG channels.** Subject average of log-ratios between stimulus and baseline of time-frequency transformed virtual channels, obtained using LCMV beamforming (2×2 virtual channels for low and high frequencies and both hemispheres separately). Only the right hemispheric channels are shown. The white empty square indicates the data points that were included in the combined EEG-fMRI analyses. Average reaction time and stimulus onset are indicated by a continuous or dashed white line respectively. **C) Average t-value distribution.** Surface projection of average t-map of the first level contrast for the general fMRI activation (top) and the contrast between left and right stimulus orientation (bottom) for illustrative purposes.

EEG data processing

The major goal of the EEG data preprocessing was to optimize noise suppression for each frequency band of interest (α, γ) in order to extract EEG signal components of interest as clean as possible. In previously published literature a supervised signal decomposition based on ICA has been utilized [18, 31]. This approach requires the manual selection of target components for each frequency band. By removing all non-target components, noise can be suppressed and the resulting signal will only contain the data of interest. However, beamforming offers the major advantage of being able to perform unsupervised noise suppression [69, 70]. During the piloting phase, beamformer methods were successfully applied to the EEG data collected in an (f)MRI environment and yielded accurate source reconstruction results, in line with previous studies using a similar approach [71, 72].

Low (α) and high (γ) frequency bands were processed separately to extract the desired response patterns. The data was filtered for the lower frequencies using a pass band between 2 and 32 Hz and for the high frequencies between 20 and 120 Hz respectively. A 50 Hz dft filter to suppress power line noise was applied to the latter as well. EEG electrode locations were obtained from the photogrammetry based 3D model and co-registered using the face shape to the anatomical MRI using janus3D, as described in Clausner et al. (2017) [43]. A finite element model (FEM) was computed from the high resolution anatomical T1 based on the FieldTrip-SimBio pipeline [73]. The leadfield was computed from the EEG electrode positions and the FEM model. Sources were modelled as equivalent current dipoles at locations limited to the respective coordinates of voxels included in the gray matter and ROI masks. Dipole orientations were derived from the cortical curvature and thickness, since this is crucial for a precise mapping especially in EEG [74]. Workbench [63] was used to compute the surface normals that connect pial and white matter surfaces. The orientation of the resulting vectors then served as the dipole orientation for each respective location. The described procedure was done separately for the left and right hemisphere in order to obtain separate filter weights, since distinct source activity for both hemispheres was to be expected [75]. The resulting weight matrices were applied to the band pass filtered data in order to obtain virtual channels at the corresponding equivalent current dipole locations. A spectral analysis was performed on each virtual channel separately. Thereby the exact settings for low and high (time-) frequency decomposition varied slightly. While for low frequencies, a Hanning taper was applied using a data time window length of 400 ms (time steps: 20 ms), zero-padded to achieve a frequency resolution of 0.5 Hz and smoothed with a kernel width of ± 2 Hz; for high frequencies the data was processed using the same time related settings, applying a multi-taper (DPSS [76]) approach (seven tapers) with a resolution of 2.5 Hz. The frequency domain was smoothed using a kernel width of ± 10 Hz. Afterwards the virtual channel with the highest average amplitude change between $8 - 12$ Hz (α) or $50 - 70$ Hz (γ) relative to baseline, was selected. As a baseline period, a time window from -0.3 to -0.1 s for high and at -0.3 for low frequencies was chosen. Gradient artifacts caused by ringing of MRI machine's amplifier after the gradient coils were switched off were observed prior to -0.3 s relative to stimulus onset which was unexpected. The initially planned start of the baseline period was -0.5 s, however due to those artifacts -0.3s relative to stimulus onset served as the new lower bound for the baseline period. For this reason, the low frequency baseline period comprised only a single time point at -0.3 s, because a pre-stimulus α decrease was expected starting around 0.25 s prior to stimulus onset. Pre-stimulus α has often been related to visual detection performance [77] and might thus reflect different processes than the actual target time interval. In fact a small but visible α decrease could be observed 0.25 s prior to stimulus onset (see Figure 2 B, top). The data was transformed into the $\log_{10}$ ratio between the baseline and each sample

point in a time window between 0.1 and 1.6 s after stimulus onset for each hemisphere. The time-frequency (TF) transformed virtual channels with the highest average response were chosen to be the "best" channels that were later used to build the regressors for the combined EEG-fMRI analyses. In total four dipole locations (i.e. the TF transform of corresponding virtual channels) were selected for each subject individually: One for each of the two hemispheres and one for each of the two separate frequency bands. Figure 2 A depicts the result of a full-brain DICS beamformer analysis [78] for illustrative purposes. Since the LCMV beamformer approach was limited to specific ROIs obtained from pRF mapping, the DICS full brain scan was performed in order to verify that indeed visually induced activity yields the strongest effects at the occipital pole. All steps previously mentioned were implemented in MATLAB R2021a [79] using the open source toolbox FieldTrip. See Figure 2 B for a depiction of the average TF transformed virtual channel response over participants for one hemisphere and both frequency bands. Since the main hypotheses of the presented study do not directly address the frequency responses (i.e. power changes) themselves, which are well established response patterns, but rather their relation to the BOLD signal, a pre-selection of EEG data with the strongest response, still acts as valid scientific strategy and does not result in a case of "double dipping".

Combined EEG-fMRI analysis

The general logic of fitting trial-by-trial based EEG time-frequency regressors individually for each TF bin to the BOLD signal for different cortical regions and across layers, follows largely what is described in Scheeringa et al. (2016) [18]. Several steps have been undertaken to prepare the EEG and fMRI data for the later combined analysis.

Nuisance regressors contained all trial and response combinations that were not included in the task regressors (e.g. false alarm trials). Additional regressors contained blink or artifact trials, button presses and reaction times. All the aforementioned regressors were convolved with the hemodynamic response function as built into SPM12. Reaction time regressors were treated as a parametric modulation. The onset of the modulation was set to the average reaction time for each individual block and the actual reaction time as the modulating value. This procedure was chosen in accordance with previous literature [18]. Furthermore the average white matter signal and the average residual signal (average signal after regressing out gray and white matter signals) were included in the nuisance regressor matrix. All motion parameters (translation along and rotation around x, y, z) and their first derivatives were included as well as a set of high pass filters modelled as five sines and five cosines. Those five sine and cosine waves were constructed, such that they would span one to five full cycles across one experimental block. **Task related fMRI regressors** were built separately for left and right oriented gratings or both combined.

EEG data regressors were built on the TF resolved virtual channel data, obtained as described above. Frequency bin span 0.5 Hz for low and 2.5 Hz for high frequency data and time bins were set to 0.4 s that were shifted by 0.1 s intervals (sliding window). One regressor was built for each frequency and time bin separately. This was done by convolving z-transformed trial-by-trial power changes of the EEG data with the hemodynamic response function that comes with SPM12, such that each regressor served as parameter modulator. Thereby the time onset was set to the mid data point of the time domain data bin and shifted by one to three TRs matching the corresponding three volumes that have been recorded after the corresponding trials. In the later general linear model (GLM) each TF based regressor was fit in a separate model. Task and nuisance fMRI regressors however were kept fixed for each model. Similar to fMRI based task-regressors, three sets of task-related regressors were built for left or right oriented trials and both combined. All analyses were performed for a (EEG) time window ranging from 0.1 s to 0.8 s after stimulus onset, for which corresponding time bins were averaged. This was done because the average reaction time to oddball stimuli was 759 ms. Since the main stimulus processing is assumed to take place before the response - but in order to include as many data points as possible - the time bin including 0.8 s after stimulus onset was included as well.

Before the combined EEG-fMRI analysis could be conducted, a normalization step has been applied in order to counteract the signal drop-off resulting from the interleaved sequence. Since in each trial the gap was followed by the collection of 3 consecutive volumes, each voxel of such volumes within one block was divided by the average BOLD signal in that voxel of every 1^{st}, 2^{nd} or 3^{rd} volume in that block. Furthermore, a first level fMRI analysis on the motion corrected data was performed in order to identify **voxels of interest**. Thereby multiple selection criteria were applied to the first level t-maps: The *feature unspecific* BOLD response (fu) is defined as the response to any stimulus (irrespective of orientation). The *feature specific* BOLD response (fs) in turn is defined as the response of a voxel to a specific stimulus orientation compared to baseline or the contrast between both ($left - right$ stimulus orientation). A positive t-value from the contrast thereby indicates a stronger response to left over right oriented gratings, whereas a negative t-value reflects a voxel's response preference to right oriented gratings. This allows the formation of a joint selection to group voxels based on the feature specific response compared to baseline *and* the contrast. A voxel with e.g. feature specific BOLD increase ($t > 0$ for the right stimulus compared to baseline) and negative contrast value ($t < 0$) to that same stimulus would be said to be a) generally activated by the right stimulus and also stronger compared to the left stimulus (explained in detail below). As the threshold used for voxel selection was inconsistent in the previous fMRI-EEG publications, we decided to adopt a transparent approach. Each selection was made such that the top 5%, 10% and 25% of voxels (according to t-value) were included. We corrected for multiple comparisons accordingly (see below). See Figure 3 C for a visual representation of the analysis strategy, Table 1 for a summary of the used nomenclature.

Importantly, fMRI based voxel selection and EEG based trial-type related regressors could either be combined congruently or incongruently (since feature specific response and the feature contrast can be divided into responding stronger to the left or right oriented stimuli). This means that results could be selected for data of all voxels that respond feature specific to one orientation with EEG based regressors built on trials of exactly this orientation (congruent; short: EEG_{co}) or the respective other orientation (incongruent; short: EEG_{inco}). A congruent pairing (EEG_{co}) would e.g. combine data of each voxel with a stronger BOLD increase

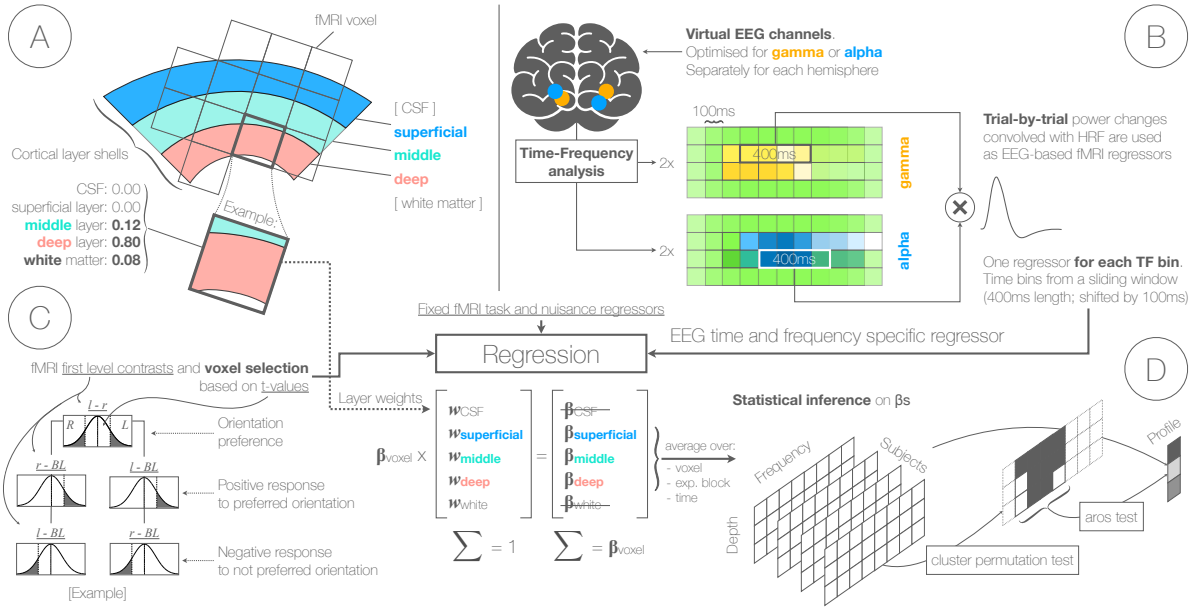

Figure 3: **Data preparation and combined EEG-fMRI analysis** for three cortical layers. **A) Layer specificity.** Cortical layers are constructed as shell-like meshes, taking the gray and white matter boundaries as reference. Between those two reference shells two additional shells divide the space between gray and white matter into three layers. The area outwards relative to the gray matter boundary is assigned to the CSF layer, whereas the area inwards from the white matter boundary is assigned to the white matter layer. Each voxel contributes a fraction of its signal to those layers, depending of the proportional volume of a voxel within each shell like mesh of each layer (see example). Respective fractions are later used as weights to split the β coefficients resulting from GLM into different layer contributions. **B) EEG based regressors.** After transforming the EEG data into virtual channel data for each grid point within the gray matter (using LCMV beamforming), virtual channels are time-frequency transformed. For each hemisphere and frequency band separately (2 Hz to 32 Hz for α and 20 Hz to 120 Hz for γ) the virtual channel with the highest γ power increase or α power decrease after stimulus onset is selected respectively ($\sum = 4$ virtual channels). Regressors are build for each time-frequency bin separately. Time bins are averaged to boost SNR. Power values over trials are convolved with the HRF as built into SPM12 resulting in one parameter modulation regressor for each TF bin. **C) Voxel selection.** Voxels are selected based on t-maps resulting from first level contrasts. Thereby, both stimulus orientations vs baseline, each stimulus orientations vs baseline or the contrast between both orientations are considered. **D) Statistical inference.** EEG based regressors are entered into a general linear model (GLM) as predictors for the BOLD signal in each selected voxel. The resulting β coefficients for each voxel are multiplied with the respective layer weights (excluding white matter and CSF layers) in each voxel and averaged for the respective time window of interest (0.1 s to 0.8 s after stimulus onset) to obtain the final depth by frequency resolved data. This data was tested against the hypothesis that there was no significant relationship between the EEG and fMRI data (β coefficients do not differ from zero) for each respective condition, using a cluster permutation test [80]. Resulting clusters were averaged in each layer over frequencies for the widest possible window selected across layers. The layer profiles of the averaged clusters were tested against the hypothesis that the layer profile is as likely as any other layer profile - under the assumption of interchangeability of the data - using an auto-regressive rank order permutation (aros) test [81].

to left with EEG based regressors based on trials where the stimulus orientation was left. In the case of EEG_{inco}, the same feature specific voxels would rather be combined in a selection with EEG-based regressors for right oriented stimuli. If voxels for both orientations have been selected (feature unspecific response) an EEG regressor that was built on both trial types was used in the result selection (no congruence separation).

Irrespective of voxel selection, a higher **t-value selection threshold** indicates higher specificity for the respective stimulus and a lower threshold increases the signal-to-noise ratio (SNR) by including more data. This changes the number of voxels selected. In previous publications, employing a similar experimental setup, 500 voxels with highest activation [82, 83] or the top 5%, 10% or 25% activated voxels [18] were selected. A study by Markuerkiaga et al., specifically designed to assess the number of voxels required for optimal SNR in the context of laminar level fMRI, finds 250 voxels (for 3T fMRI) to yield the best contrast-to-noise ratio (CNR) [84]. However, since all previously mentioned publications set a more or less arbitrary threshold and the last did not take the correlation with EEG into account and hence potential changes in SNR and CNR for those cases, three thresholds have been selected to eliminate eventual uncertainties: 5%, 10% and 25% of most activated voxels.

A **general linear model** (GLM) has been computed with predictors for each TF bin separately for all voxel in V1 that later have been sub-selected according to the respective condition. Afterwards, each of the resulting regression coefficients (β coefficients) was multiplied with the voxel specific layer weights that have been obtained as described above. The general strategy rests on the idea that the predicted fMRI activity can be seen as a mixture of signal contributions from each layer in each voxel. For this analysis, contributions from white matter and CSF layers have been excluded and only signal contributions from superficial, middle and deep layers have been taken into account. After averaging results from different hemispheres, experimental blocks, percentiles of interest (e.g. the top 5% voxels of a respective contrast) and time bins for a time interval between 0.1 and 0.8 s after stimulus onset, the final data contains the average regression coefficients for $depth \times frequency \times subject$.

Subsequently, separate analyses were done for two frequency of interest (FOI) ranges centred around the α and γ band responses observed in the EEG. Within these frequency ranges **inferential statistics** based a cluster level approach were computed. For low frequencies the FOI range was set to frequencies between 8 Hz and 14 Hz (α band), whereas

for the high frequencies the FOI was defined as frequencies between 50 Hz and 70 Hz (γ band), which covers the peak response frequencies found in the average EEG data (see Figure 2 B). Within the respective range - and if not otherwise indicated - a single tailed cluster permutation test [80] has been conducted separately for each threshold and FOI for α and γ in V1 since the expected direction of the effect was derived from the literature [18, 85, 86]. Each significant cluster has been further processed by means of an auto-regressive rank order similarity (aros) test [81]. The fundamental idea behind the aros test is whether group averages (i.e. averages of the signal of cortical layer in the present case), can be ranked such that the rank order is explained significantly better by the data than it would if the average data could not be meaningfully sorted (i.e. is shuffled). This is achieved by transforming the group averages into unique rank order values (e.g. superficial > deep > middle) and computing the average fit of the data to this rank order. In a second step data points are shuffled between the groups and the same procedure is applied (i.e. computing the rank order of the mean and the average fit of the now shuffled data to the new rank order). Repeating this permutation step a large number of times (here 25000 times) yields a permutation distribution, to which the initially computed fit value of the un-shuffled data is compared. Rejecting the null hypothesis would result in the assumption that the rank order of the group averages indeed can be explained by the data significantly better than it would if the data points could not be meaningfully sorted into those groups. Thus, in the present case it could reveal how the correspondence between the EEG and fMRI signals could be sorted across layers. However, statements about the magnitude of the difference between two (or more) layers cannot be made. This approach provides insight about the specific activation profile across layers for specific conditions within a significant $depth \times frequency$ cluster. Since clusters span layer and frequency bins unevenly, the data that was used for the later aros test was collapsed over frequencies, such that the lowest and highest significant frequency bin served as the boundary over which the frequency domain was averaged. This was done irrespective of the respective cluster size within a specific layer (see Figure 3 D). Testing for layer specificity is not straightforward due to issues related to multiple comparison and non-normal distributed data. To circumvent this, Scheeringa et al. (2016) [18] tested for EEG-fMRI layer specificity by fitting layer profiles for α and γ to each other using an ordinary regression and tested whether β coefficients differed to zero. While this approach is suitable for demonstration purposes, it does not reveal the exact nature of those differences between layers. While Scheeringa et al. proved the concept of layer specific feature extraction, the present paper aims to determine the relational activity across layers depending on the feature specific response as well for which reason the aros test has been developed. For the present case this means that while neglecting the effect size of the difference across layers, the overall profile of the differential activation across layers can be obtained without compromising statistical power due to multiple comparison.

The described procedure of selecting the respective voxels of interest, fitting EEG based regressors jointly with task and nuisance fMRI regressors to the data, weighting the resulting β regression coefficients with the corresponding layer contribution weights and applying a cluster permutation test, followed by an aros test on significant clusters, has been applied to each of the contrasts of interest. To account for multiple comparison across the respective selection thresholds, cluster and aros p-values have been adjusted using the false discovery rate (FDR) adjustment procedure proposed by Benjamini & Hochberg [87]. In the next section, we describe the different voxels selections applied (see Table 1).

Feature unspecific BOLD decrease

Previous literature on the relationship between laminar level fMRI and EEG in the visual domain mainly focused on proofs of concept and related visual cortex fMRI activity to EEG without considering different stimulus features [18, 31], which has been accomplished here. Furthermore, the relationship between visual cortex fMRI data and EEG has been extended to include visual cortex *deactivation*. In general, the sparse corpus of literature investigating negative fMRI deflections in conjunction with the presentation of visual stimuli mainly focused on attention related effects [35, 88] (especially for foveal presented stimuli and a demanding task; see Crespi et el., 2011 [89]). Furthermore, it has been related to decreased neuronal activity in monkey V1 [36]. Note, that attention was not manipulated as part of the experimental setup. The results in Figure 2 C (top half) however, strongly suggest some attention related processing being involved, as the pattern largely matches what has been reported for retinotopic activation patterns under the involvement of spatial covert attention [35]. More specifically, the observed pattern suggests an upwards directed attention bias, which has been reported in previous literature as well [90], especially for object (and not spatial) based stimulus judgements [91], as was the case for this study. Strikingly, the clear separation between positive and negative t-values for both stimuli (see Figure 2 C bottom) along the calcarine fissure disappeared when contrasting both stimulus orientations (presumably because attention related and other general effects do not vary depending on the stimulus orientation). The positive BOLD signal component is expected to reflect the feature specific response under the influence (enhancement) of attention [85]. Hence a strong entanglement of attention for receptive fields and feature related processes (when conducting the analysis for both stimuli combined) is expected. To overcome this limitation and identify "true" feature-unspecific signal components, we have focused on the negative feature unspecific BOLD signal to rule out feature specific contributions, because at attended locations, the BOLD signal inevitably comprise feature related signal components. In addition, previous literature suggests that attention related α power increases could be associated with BOLD-signal decreases [35, 36, 85] and hence might provide a meaningful insight into feature unspecific signal contributions. As described above, for each contrast, multiple thresholds have been applied such for voxels with the 5%, 10% and 25% most negative t-values.

Feature specific BOLD response

In general, the response to the two orthogonal stimulus features has been assessed two fold. Based on the t-value obtained from the first level contrast ($left-right$ stimulus orientation), and by comparing the t-values of one orientation to baseline. For the first case, voxels respond preferentially to one *over* the other orientation. The result of the contrast and the response compared to baseline then create a joint selection. This is the response of a voxel to one stimulus orientation compared to baseline, relative to the response of that voxel to the other stimulus. Hence, voxels with a

contrast value that is based on the difference between one positive and one negative or two negative values compared to baseline are systematically excluded. This joint selection between feature specific voxels with strictly positive response compared to baseline, can be interpreted as **feature specific BOLD increase**. In turn, feature specific BOLD decreases could be defined accordingly, but because of how the feature contrast is defined (stronger response to one orientation *over* the other orientation), the **feature specific BOLD decrease** was solely based on the comparisons to baseline. This means that a feature specific BOLD decrease to one orientation includes those voxels that have a stronger BOLD decrease compared to baseline as compared to the other stimulus orientation compared to baseline, but only for those voxel with a t-value smaller than zero. Lastly, voxels were selected based on the contrast and on whether they exposed a sign flip as a result of being presented with one or the other orientation. While the feature contrast does not limit the voxel selection based on a voxel's response compared to baseline, and the feature response compared to baseline limits the voxel selection to either positive *or* negative responses compared to baseline, the **feature specific BOLD sign flip** response is formed by a joint selection of contrast value and whether a voxel responds with a BOLD increase to their preferred orientation *and* with BOLD decrease to the respective other orientation. Using this procedure an indirect link between feature specific inhibition in the context of feature processing can be established. See Table 1 for a summary of all conditions.

Each selection can be further split into voxels that respond preferentially to $left$ or $right$ stimuli. In addition, the EEG regressors can as well be separated into $left$ and $right$ by the trials they were constructed from. Using this strategy, the result of the GLM can be separated into congruent or incongruent parts, were feature specific signal changes were assessed for congruent (EEG_{co}) or ingongruent (EEG_{inco}) combinations of selected voxels and EEG based regressors. Beside separately looking at congruent and incongruent combinations, contrasts have been computed as the difference of β coefficients between EEG_{co} and EEG_{inco} ($EEG_{co-inco}$). Here, attention related effects are assumed to not play an important role, since the same sub-selection of voxels was used and a bias resulting from orientation dependent EEG regressors with respect to attention appears very unlikely. As previously mentioned, each set of results was followed by a single tailed cluster permutation test [80]. The only deviation to this is the test on feature specific sign flip data, with EEG_{inco}. Here a two sided cluster permutation test has been performed, because the directionality of the effect could not be reliably derived from the literature or theoretical models.

The final results structure encompasses the layer by frequency resolved data for each voxel selection threshold and combination with EEG power regressors, significant clusters and aros results for α and γ separately. Figure 4 provides a dummy result figure with explanations on the arrangement of plots. Furthermore, results averaged over frequencies within each cluster can be found in the supplementary material.

description	pref. ori.	selection criteria
feature unspecific BOLD decrease (*fu decr.*)	–	$[stimulus - BL] < 0$
feature specific BOLD increase (*fs incr.*)	L	$[l - r] > 0$, with $[l - BL] > [r - BL] > 0$
	R	$[l - r] < 0$, with $[r - BL] > [l - BL] > 0$
feature specific BOLD decrease (*fs decr.*)	L	$[l - BL] < [r - BL] < 0$
	R	$[r - BL] < [l - BL] < 0$
feature specific BOLD sign flip (*fs flip*)	L	$[l - r] > 0$, with $[l - BL] > 0 > [r - BL]$
	R	$[l - r] < 0$, with $[r - BL] > 0 > [l - BL]$

Result combinations	pref. ori.	EEG regressor
congruent (EEG_{co})	L	EEG_L
	R	EEG_R
incongruent (EEG_{inco})	L	EEG_R
	R	EEG_L

Table 1: **Contrast dependent voxel selection** Voxel selections were made based on t-maps resulting from first level fMRI analyses. Those t-maps include any stimulus compared to baseline ($stimulus - BL$), the contrasts between both stimulus orientations (i.e. $left - right$ or $l - r$) and each stimulus separately compared to baseline ($l - BL$ or $r - BL$). From those four t-maps, voxel selections have been derived to answer respective hypotheses. Depending on the respective selection threshold voxels can be further sub-selected (e.g. top 5%). The *feature unspecific BOLD decrease* has been assessed by selecting the data of voxels with a general BOLD decrease to any stimulus irrespective of the stimulus orientation. *Feature specific BOLD increase* was defined as those voxels that were separated based on the sign of the contrast $l - r$, which was further sub-selected to only contain voxels that are strictly positive when comparing each stimulus to baseline. *Feature specific BOLD decrease* in turn is assessed by separating voxels into L and R depending on the stimulus orientation for which the t-value of the stimulus compared to baseline is most negative and excluding voxels with a t-value (≥ 0). Lastly, voxels have been analysed that expose a *feature specific BOLD sign flip*. Those are voxels that have been grouped into L and R based on the feature contrast and were sub-selected such that the response to one orientation compared to baseline is positive, while the response to the respective other orientation compared to baseline is negative. After computing the GLM, the result matrices were obtained by grouping β weights for the respective voxel selections (L or R) and EEG regressors either congruently (EEG_{co}) or incongruently (EEG_{inco}) with the stimulus orientation of the trials the EEG based regressors were built from.

Results

Behavioral data and basic task effects

Behavioral and basic task effects were only analyzed descriptively. No inferential statistics have been conducted, since those analyses mainly served as sanity checks or re-

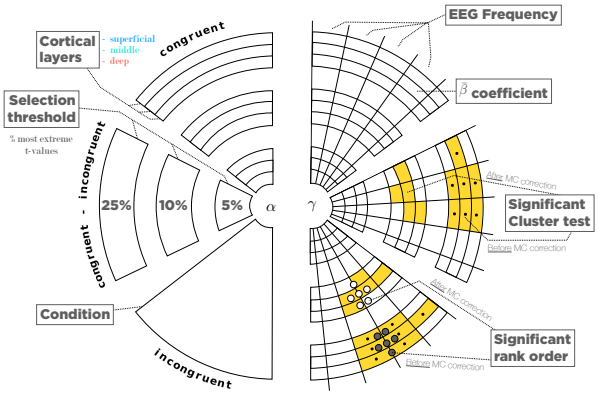

Figure 4: **Composition of result figures.** The main result plots will be composed of 6 "slices" or "pieces of cake", where each "slice" represents one congruence condition. Each slice will look like the bottom right one in this figure. For illustrative purposes the information is built up clock-wise starting at the bottom left slice. The left hand slices reflect the results for the α band and the right hand side results for the γ band, while the top two slices reflect *congruent* and the bottom two reflect *incongruent* results. In between (centre) the contrast *congruent* − *incongruent* can be found. Each shell-like structure reflects a certain selection threshold with results where t-values used for voxel selection that are most extreme are located towards the centre (e.g. top 5%). Each of the threshold shells is again sub-divided into three layers, reflecting (from outside towards centre) superficial, middle and deep layer results. At the outer ring the respective frequency is shown. A cluster permutation test has been performed on each layer by frequency "patch" and significant results are highlighted using more saturated colours. If a cluster failed to reach significance after correction for multiple comparison, the cluster is decorated with tiny black dots. In case of a significant cluster (before correction for multiple comparison), an aros test has been performed, to determine the rank order the effect across layers. Thereby, three dots (○ ○ ○) indicate the strongest and one dot (○) the weakest effect in case the test reached significance. Again, if an aros result did not reach significance after multiple comparison correction or in case the aros test was performed on a cluster that did not reach significance after multiple comparison correction, the aros result is shown as black dots (rather than white). Hence, statistically most relevant effects will be reflected in highlighted clusters without black dots and white circles indicating the rank order across layers.

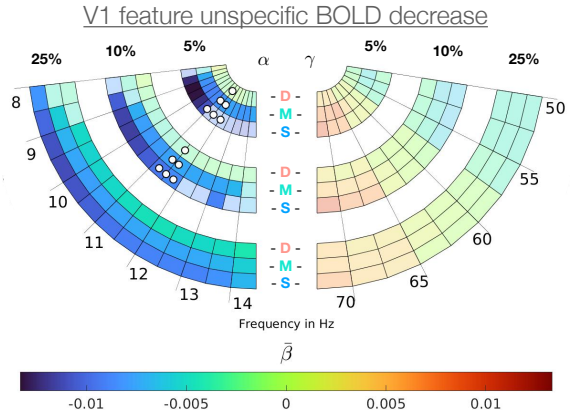

Figure 5: **Average β coefficients** (average contribution per voxel) for voxel sub-selections with negative t-values for both stimulus orientations combined (general activation). For each frequency bin a separate model has been computed and results were weighted with the respective layer contribution weights. Frequency bins (0.5 Hz steps for α and 2.5 Hz steps for γ) are indicated at the out-most half circle. Layers are indicated by coloured abbreviations for superficial (S), middle (M) and deep (D) layers. Percentages indicate the threshold at which voxels were selected (e.g. 5% would refer to the 5% most negative t-values given a respective sub-selection). More saturated areas indicate a significant cluster after a cluster permutation test [80]. For each significant cluster an aros test [81] has been conducted across all layers for the widest possible frequency range that the cluster spans. In case of a significant result, white circles indicate in which layers the respective effect was strongest (3 circles), medium strong (2 circles) and weakest (1 circle). Thereby, the strongest effect in the α band corresponds to the most negative β values. Corresponding cluster and aros p-values are shown in Table 2.

flect intermediate results that were used for the main analyses. The main purpose of these analyses was to verify subject's compliance to the task (behavioral results) and expected functional result patterns (e.g. expected EEG time-frequency responses). The shown results represent the data as it was used to conduct the final combined EEG-fMRI analyses.

On average (SD) participants responded correctly to the stimuli in 94% (8%) cases with a false alarm rate of 2% (3%) to non-oddball stimuli and a miss rate of 5% (7%), indicating that participants performed the task adequately well and complied to the task instructions. The average (SD) reaction time was 759 ms (131 ms). See Figure 1 for a graphical representation of the task.

The EEG signal, used to construct regressors for the final combined EEG-fMRI analyses, was obtained by a time frequency analysis of each virtual channel, computed for each voxel location of the gray matter in V1. In each hemisphere, one virtual channel for low and one for high frequencies was selected that showed the strongest α decrease and γ increase respectively. Figure 2 B depicts the average EEG response of the selected, TF transformed virtual channel averaged over all trials and subsequently over all participants. For demonstration purposes, only low and high frequency channels of the right hemisphere are shown. By visual inspection, the main α band decrease was determined to last from 0.2 s to 0.8 s after stimulus onset and for a frequency range of 8 Hz to 14 Hz. The main γ band increase was determined between 0.1 s and 0.7 s after stimulus onset for a frequency range between 50 Hz and 70 Hz. A time window between 0.1 s and 0.8 s, was used for the main analyses, since both time windows for α and γ responses are covered. Furthermore, this time window ensures that only time bins went into the analyses that were related to the actual stimulus processing (μ_{RT} = 759 ms), but at the same time that the signal-to-noise ratio was kept as favourable as possible. To verify that the main TF response of interest originated at the occipital pole, a DICS beamformer full brain analysis had been conducted at the centre frequencies of the selected bands. As visible in Figure 2 A the top 5% of the subject averaged strongest decrease at 11 Hz or increase at 60 Hz in response to the stimulus indeed localized to occipital regions.

While the result of the general activation first level BOLD analysis (both stimulus orientations) within V1 showed a clear-cut t-value distribution pattern around the calcarine sulcus with more negative t-values located dorsal and more positive t-values ventral to the fissure, the first level contrast between both stimulus orientations did not. However, a similar pattern as observed with both stimulus orientations has been found for each stimulus orientation separately compared to baseline. In addition to the observed distribution of positive and negative t-values, the peak activation for any or both stimuli compared to baseline were expected to locate to the occipital pole, due to the central presentation of the stimulus [53, 92]. When computing the contrast between both orientations, this peak should be much less pronounced

or absent. Both of those patterns have been observed. See Figure 2 C for a visual representation. Again, this visualization only serves descriptive purposes. No inferential analyses have been conducted.

Combined EEG-fMRI analyses

The relationship between the EEG and fMRI data has been investigated on a trial-by-trial basis by means of a general linear model (GLM) as done previously [18, 31]. A separate GLM model was computed for each TF bin by convolving the EEG response of time-frequency transformed virtual channels with the standard hemodynamic response function as built into SPM12. Task and nuisance fMRI regressors served as control parameters and were fixed for each model. β coefficients for every voxel that were taken into consideration were multiplied by the layer weights for those respective voxels. This procedure was repeated for multiple activation thresholds used to select a respective sub-set of voxel, such that the most activated (or deactivated) 5%, 10% and 25% voxels have been considered. The data was averaged for a time window between 0.1 s and 0.8 s after stimulus onset. Here, only results for V1 are reported, mainly due to poor data quality of the pRF mapping, which resulted in less distinguishable higher order visual areas (V2, V3). Additionally, the used stimulus material specifically targeted high activation in V1 (over V2 or V3) [93]. Results for V2 and V3 are reported in supplementary material (see Figures Sf1, Sf2, Sf3 and Sf4 and Tables St2 and Tables St3) and do not substantially deviate from results for V1.

Feature unspecific BOLD decrease

A significant negative relationship between low frequency EEG (α) power changes and negative BOLD signal deflections (i.e. the more negative the BOLD, the stronger the α) irrespective of trial type has been found using a cluster permutation test [80] for all three sub-selection thresholds (5%, 10%, 25%) for each of the selected sets of voxels. See Figure 5 for a visualization of the results and Table 2 for for p-values, corrected using the Benjamini-Hochberg approach [87] to adjust false discovery rates (FDR). Results for V2 and V3 are shown in Figure Sf1 and Tables St2 and St3 (supplementary material). For each cluster the average data that was used compute the aros test [81] can be found in the supplementary material as well (Figures Sf5, Sf8 and Sf11).

The strongest negative relationship between α and the negative BOLD signal was found mainly in superficial layers, where main driver of this effect appear to be lower frequency α oscillations (< 11 Hz). This observation becomes even more pronounced for lower thresholds, where despite a reduced number of voxels the effect becomes stronger.

In turn, for none of the voxel sub-selections a significant effect for the high frequency (γ) EEG power regressors has been observed, irrespective of the respective selection threshold.

Feature specific BOLD response

Feature specific BOLD signal deflections have been related to EEG based regressors for (1) voxels that exhibited a feature specific BOLD increases (2) voxels that exhibited a feature specific BOLD decreases, and (3) voxels that respond positive to one but negative to the other stimulus orientation (feature specific sign flip; see Table 1). Thereby, voxels with stronger response to the $left$ or $right$ orientation (for negative responses this means a stronger negative deflection) have been combined with EEG power regressors (for α or γ separately) built from $left$ or $right$ oriented trials, either congruently (EEG_{co}) or incongruently (EEG_{inco}). Furthermore, the contrast $EEG_{co-inco}$ has been computed for each respective sub-selection of voxels (5%, 10%, 25%). See Figure 6 for a visualization of the results and Table 2 for exact p-values, corrected using the Benjamini-Hochberg procedure [87] to adjust false discovery rates (FDR). The result of the feature contrast alone, as well as results for V2 and V3 are shown in Figure Sf2, Figure Sf3 and Sf4 as well as Tables St1, Tables St2 and St3 (supplementary material). For each cluster the average data that was used to compute the aros test [81] and can be found in the supplementary material too (Figures Sf7, Sf10 and Sf13).

Feature specific BOLD increases (Figure 6 A)

We observed a negative relationship between the **alpha frequency** band and the feature specific BOLD signal increase for EEG_{co} . A trend level result (significant uncorrected for multiple comparisons) for feature specific, positive BOLD and EEG_{inco} was observed as well. No significant effect was observed for the contrast $EEG_{co-inco}$ in the α band. Interestingly, the exact α frequency range differs between the selection of voxels for EEG_{co} and EEG_{inco}. The exact α frequency spectrum was slightly biased upwards ($\approx$ 10 to 14 Hz) for EEG_{co} while the frequency range involved for the trend level result for EEG_{inco} tend towards the lower end of α ($\approx$ 8.5 to 11 Hz).

The laminar profile for EEG_{co} has been observed to be flat with the exception of the most liberal threshold (25% most activated voxel) where the strongest relationship between α and the BOLD signal was located in superficial layers followed by deep layers. For the trend level clusters in EEG_{inco} the strongest effect was found in deep layers.

Within the **gamma frequency** range we observed a positive relationship between the γ band EEG signal and the feature specific BOLD signal increases for the contrast between congruent and incongruent conditions for frequencies between ≈ 55 and ≈ 65 Hz. Only for the most liberal threshold (25%) a significant layer profile was obtained, with the strongest relationship between γ and the BOLD signal in superficial and deep cortical layers.

Feature specific BOLD decreases (Figure 6 B)

We also observed a significant negative relationship between **alpha frequencies** and feature specific BOLD signal decreases for EEG_{inco}. Similarly to feature specific BOLD increases selection, we did not observe significant differences for the contrast $EEG_{co-inco}$ in the α band. The frequency range involved for EEG_{inco} appeared to be broadband (covering almost the entire spectrum). The laminar profile for orientation specific BOLD signal decreases voxels was found to have a stronger relationship between α and superficial and middle layer BOLD activity.

No significant results was observe for the **gamma frequency** based EEG regressors for these selections of voxels.

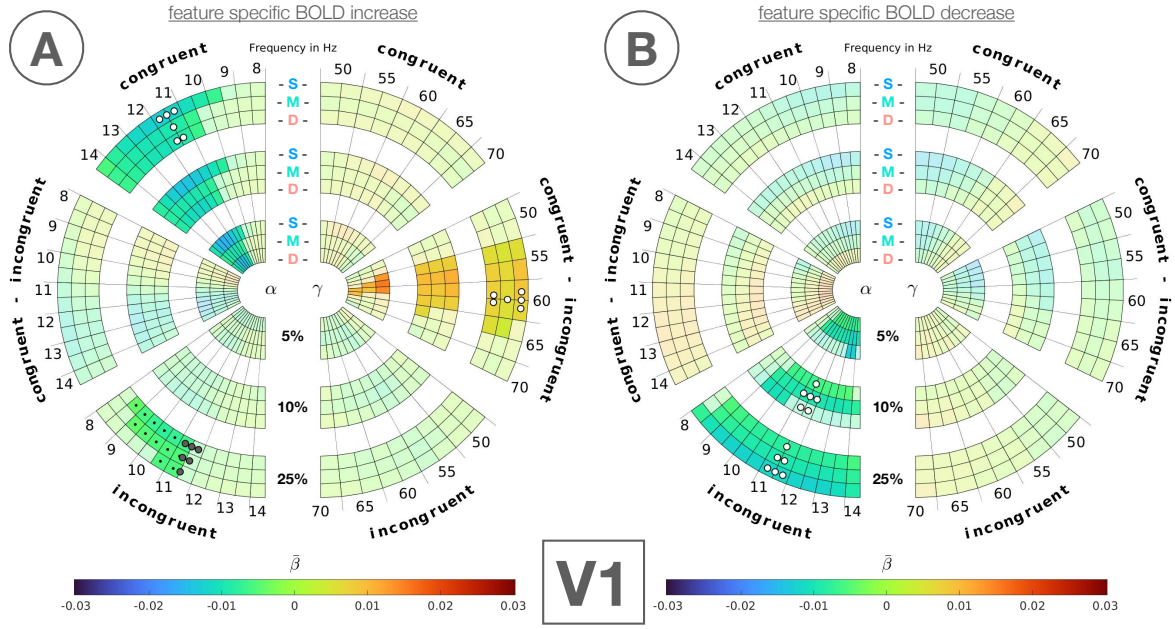

Figure 6: **Average β coefficients** (average contribution per voxel). For each frequency bin a separate regressor has been used and results were weighted with the respective layer contribution weights. Frequency bins (0.5 Hz steps for α and 2.5 Hz steps for γ) are indicated at the out-most half circle. Layers are indicated by coloured abbreviations for superficial (S), middle (M) and deep (D) layers. Voxels were selected based on the first level fMRI contrast as follows: **(A)** Voxels that respond strictly positive to both orientations and stronger to one orientation over the other or **(B)** Voxels that respond more negative to one orientation compared to baseline as the other orientation compared to baseline does. See also Table 1 for an overview of how the conditions are constructed. Percentages indicate the threshold at which voxels were selected and refer to the respective sub-selection (e.g. 5% would refer to the 5% most positive or negative t-values given a respective sub-selection). Congruent thereby means that if a voxel e.g. responds stronger to left oriented gratings over right oriented gratings EEG based predictors for the *left* orientation trials (and vice versa) were used to compute the results. In turn incongruent means that if a voxel e.g. responds stronger to left oriented gratings over right oriented gratings based predictors for the *right* orientation trials (and vice versa) were used to compute the results. More saturated areas indicate a significant cluster after a cluster permutation test [80] and FDR correction [87]. Black dots indicate a cluster p-value of $> .05$ after, but $< .05$ before the correction was applied. For each significant cluster an aros test [81] has been conducted across all layers for the widest possible frequency range that the cluster spans. In case of a significant result after FDR correction, white circles indicate in which layers the respective effect was strongest (3 circles), medium strong (2 circles) and weakest (1 circle). If the aros p-value was $< .05$ before, but $> .05$ after the correction, aros shapes are indicated using grey circles. The strongest effect in the α band corresponds to the most negative β values, whereas in the γ band the strongest effect refers to the most positive. Corresponding cluster and aros p-values are shown in Table 2.

Feature specific BOLD with sign flip (Figure 7)

We observed a negative relationship between **alpha frequencies** and feature specific BOLD signal deflections that are positive for one, but negative for the other orientation for EEG_{co} and the contrast $EEG_{co-inco}$. Both showed a bias of the effect towards deep layers and while the effect for EEG_{co} spans almost the entire frequency spectrum of interest, the effect for the congruence contrast was observed to be biased towards the upper α range (≈ 10 to ≈ 14 Hz). Additionally a *positive* relationship between α and the BOLD signal was found for the deep layer in EEG_{inco} for the 5% most specific voxels.

No significant results was observe for the **gamma frequency** based EEG regressors for these selections of voxels.

Discussion

In the present study, laminar level fMRI was combined with simultaneously recorded EEG in healthy human participants. We tested whether stimulus induced changes in EEG power in the α and γ band relate to feature specific or feature unspecific neural activity at the level of cortical layers as reflected in the BOLD signal. First, we observed that γ band oscillations are positively correlated with feature specific BOLD signal increases in superficial layers as predicted by the literature [6, 8, 16, 18]. In addition to that we observed that γ band oscillations are also related to deep layer BOLD activity changes (see Figure 6 A). Second, we found α band oscillations to be negatively related to BOLD signal decreases given *any* stimulus (global modulation). Although a negative relationship between α power changes and BOLD signal increases has been previously reported ([18, 31, 85]), the relationship between α and *negative* BOLD signal deflections (see Figure 5) has not been previously reported, because stimulus evoked BOLD decreases have received less attention from previous research. Furthermore, we could show that α band oscillations were inversely related to feature specific BOLD activity as well, which has been predicted by some, but not the majority of theoretical frameworks [8] (see e.g. Figure 7). The global and feature specific relationship between α and BOLD signal fluctuations could be attributed mainly to superficial and deep layers, both layers being predicted by the literature [8, 16, 94].

We first discuss the fMRI results before moving to the combined analyses. Strikingly, in addition to a large positive BOLD response, we observed a reduced BOLD activity (independent of the stimulus orientation) dorsal of the calcarine sulcus (Figure 2 C top). Even though attention has

		V1											
		α						γ					
		5%		10%		25%		5%		10%		25%	
		cluster	aros	cluster	aros	cluster	aros	cluster	aros	cluster	aros	cluster	aros
fu decr.	-	.026	.000	.026	.000	.004	-	-	-	-	-	-	-
fs incr.	co	.006	-	.006	-	.003	.000	-	-	-	-	-	-
	co - inco	-	-	-	-	-	-	.043	-	.021	-	.021	.000
	inco	-	-	-	-	○	○	-	-	-	-	-	-
fs decr.	co	-	-	-	-	-	-	-	-	-	-	-	-
	co - inco	-	-	-	-	-	-	-	-	-	-	-	-
	inco	.011	-	.011	.000	.002	.000	-	-	-	-	-	-
fs flip	co	-	-	.007	.000	.000	.000	-	-	-	-	-	-
	co - inco	.026	-	.017	.000	.007	.000	-	-	-	-	-	-
	inco	.041	○	-	-	-	-	-	-	-	-	-	-

Table 2: **False discovery rate (FDR)** adjusted p-values, computed using the Benjamini-Hochberg procedure [87] for the respective voxel sub-selections in V1. FDR corrections where computed on the p-values resulting from either the cluster permutation tests [80] or the corresponding aros tests [81] across the respective selection thresholds (5%, 10% and 25%). The circle symbol (○) indicates a p-value smaller than 0.05 before multiple comparison correction was applied. Conditions are abbreviated as follows: **fu decr.**: feature unspecific BOLD decrease (negative BOLD for any stimulus compared to baseline); **fs incr.**: feature specific BOLD increase; **fs decr.**: feature specific BOLD decrease;**fs flip**: feature specific BOLD sign flip (feature specific positive BOLD for one orientation, but negative for the other orientation). See also Table 1 for more information and Figure 6 for a visual representation.

not been manipulated as part of this experiment, the overall distribution of positive and negative BOLD reported here, closely resembles previous findings on the retinotopy of the attentional spotlight, where attended locations would result in higher BOLD activity whereas unattended parts result in less BOLD activity [35]. One interpretation would be that the task (detecting wiggles) could be solved by spatially attending one part of the stimulus only. Those negative deflections do probably not reflect a case of "blood stealing" [58], since it has been found that a decrease in attention led to a decrease in the BOLD signal [88] as well, which could furthermore be related to decreased neuronal activity [36]. More importantly, we were able to isolate voxels with a *feature-specific* response for both positive and negative (i.e. voxels that are more negative for one orientation than the other) BOLD signal deflections. The feature-specific negative voxels might reflect sharpening through feedback [95]. However, a small portion of these negative voxels responded positively to the other orientation (flip voxels). Given the small amount of these voxels, we believe that these flip voxels are rather negatively modulated by nearby activated voxels (sharpening) through horizontal connections [96].

The combined EEG-fMRI analyses revealed a positive correlation between γ and feature-specific voxels in both superficial and deep layers. The relationship between γ and superficial layer BOLD is similar to what has been reported by Scheeringa et al. (2016) [18]. In addition to that, previous work in monkeys also attribute γ band activity to superficial layers [16]. Accordingly, oscillations in the γ band have been attributed mostly to a feed-forward flow of information via superficial anatomical connections [6, 7]. However, we also found a relationship between γ and deep layer BOLD which was not reported by Scheeringa and colleagues who reported a more evenly spread layer distribution for V1, with a trend to more superficial layers in V2 and V3. A notable difference with the results presented here is that this study did not include a contrast between congruent and incongruent features. Since the here reported deep layer γ effect is stronger compared to middle layers, we do consider this finding functionally relevant. Furthermore, even though van Kerkoerle et al. (2014) [16] discuss the γ effect with respect to superficial layer neuronal activity only, their data shows a significant peak in layer 6 as well, which might even be stronger than in superficial layers and potentially even stronger modulated by task relevance (see figures 2F and 2G in the respective publication). In fact an analysis of the relationship between the EEG signal and the BOLD signal that focused only on the feature contrast ($L-R$; independent of the comparison to baseline) revealed a trend level result with an even stronger deep layer contribution as compared to superficial layers (see Figure Sf2 in supplementary material). This strongly implies an involvement of γ oscillations in feature specific processes [5]. Since γ band oscillations are thought to be related to the ongoing *active* processing of stimuli [5, 6] or directly reflect neuronal spiking activity [23], limiting the analysis strictly to voxels with a positive t-value might have increased the SNR substantially, resulting in a stronger effect for feature specific BOLD signal increases as compared to the feature contrast alone. Recent publications on the information exchange within and between primary visual cortex areas of macaques also reported deep layer γ band activity depending on the stimulus material [97, 98]. Those publications challenge the feed-forward exclusivity of γ altogether by revealing intra-area feedback communication in V1 from layer 5 to layer 6 and layer 6 to supra-granular layers. Possibly, the relationship between γ and deep layer BOLD we observed is also related to similar processes. However, it was also shown that feed-forward connections to higher order regions do exist in deep cortical layers of macaque monkeys as well [99]. Conclusive evidence about the directionality and source of the γ related deep layer effect thus remains uncertain.

The correlative nature of the here presented approach cannot provide such insights and are likely better addressed in recordings in animal models[16]. Our data however, clearly supports the investigation of feature processing related deep layer γ band activity.

Regarding α modulation, we found a general negative relationship between α band power and the orientation - independent BOLD signal decreases mentioned above (espe-

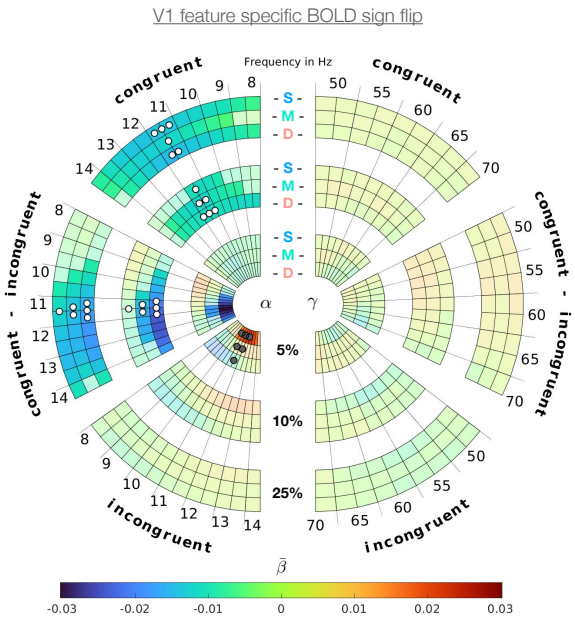

Figure 7: **Average β coefficients** (average contribution per voxel). For each frequency bin a separate regressor has been used and results were weighted with the respective layer contribution weights. Frequency bins (0.5 Hz steps for α and 2.5 Hz steps for γ) are indicated at the out-most half circle. Layers are indicated by coloured abbreviations for superficial (S), middle (M) and deep (D) layers. Voxels were selected such that they respond positive to one orientation but negative to the other orientation and stronger for one orientation as compared to the other (feature specific BOLD sign flip). See also Table 1 for an overview of how the conditions are constructed. Percentages indicate the threshold at which voxels were selected and refer to the respective sub-selection (e.g. 5% would refer to the 5% most positive or negative t-values given a respective sub-selection). Congruent thereby means that if a voxel e.g. responds stronger to left oriented gratings over right oriented gratings EEG based predictors for the *left* orientation trials (and vice versa) were used to compute the results. In turn incongruent means that if a voxel e.g. responds stronger to left oriented gratings over right oriented gratings based predictors for the *right* orientation trials (and vice versa) were used to compute the results. More saturated areas indicate a significant cluster after a cluster permutation test [80] and FDR correction [87]. Black dots indicate a cluster p-value of $>$ .05 after, but $<$ .05 before the correction was applied. For each significant cluster an aros test [81] has been conducted across all layers for the widest possible frequency range that the cluster spans. In case of a significant result after FDR correction, white circles indicate in which layers the respective effect was strongest (3 circles), medium strong (2 circles) and weakest (1 circle). If the aros p-value was $<$ .05 before, but $>$ .05 after the correction, aros shapes are indicated using grey circles. The strongest effect in the α band corresponds to the most negative β values, whereas in the γ band the strongest effect refers to the most positive. Corresponding cluster and aros p-values are shown in Table 2.

cially in superficial layers and frequencies below 11 Hz; see Figure 5). Given the general α power decrease (that would overshadow local increases; see Figure 2 A and B), we interpret this result as a reduction of decreased α power (relative increase) that would be linked to the locally reduced BOLD activity (Figure 2 C top). Future experiments manipulating attention might reveal a similar relationship between α and superficial layer cortical activity for suppressed (unattended) receptive fields. The negative relationship between α and this negative BOLD signal is in line with the hypothesized inhibitory nature of α [8, 9, 85, 100].

We observed a significant relationship between deep layer α for feature specific BOLD with sign flip (tending towards the upper α range), which stands against the traditional view of α acting as a more global modulator [9, 100] rather than a local feature-specific actor. In addition we found a significant relationship between superficial and deep layer BOLD and α (above 11 Hz) for the feature contrast voxel selection between congruent and incongruent EEG-fMRI pairings (see supplementary material). If the congruence contrast was limited to strictly positive or negative voxel, such effect was not significant. This could be explained by the limited variability if the analysis focused solely on positive or negative BOLD signal changes, where voxels with a very large response variability (e.g. strongly positive to one but negative to the other orientation) are excluded. This is in line with the results observed for flip voxels, where those highly variable voxels not only lead to the strongest effects overall (despite the number of voxels was lowest), but furthermore exposed a positive relationship between α and deep layers for feature incongruent selections. As discussed above, we believe that these flip voxels are negatively modulated by nearby activated voxels. Therefore the positive correlation between α and the negative BOLD signal could be a consequence of the negative correlation between α and the positive BOLD signal of the respective other orientation.

Interestingly, we observed that frequencies below 11 Hz were negatively correlated with the BOLD signal in the incongruent conditions of feature specific BOLD signal increases on a trend level. In the congruent condition we observed a correlation in higher frequencies of $>$ 11 Hz. Given that we observed also a stronger negative correlation for frequencies below 11 Hz with the orientation-independent BOLD signal decreases (especially for the 5% most negative voxels), we interpret the α effect below 11 Hz as a source of general modulation. Thereby, α power would possibly decrease in task-relevant pools of neurons and increase in task-irrelevant pools of neurons (i.e. attention-related). On the contrary, frequencies $>$ 11 Hz would reflect feature-specific processes, only observed in neurons responding specifically to that stimulus orientation.

The literature on differences in frequency within the α band depending on visual stimulus features is sparse. According to Klimesch (1997) [101], lower frequency α power was assumed to reflect attentional processes while upper α band power is related to semantic memory demands. Here, lower frequency α appears to be related to the modulation of negative BOLD signal changes for general (see Figure 5) processes. This would be in line with the findings on lower frequency α reported by Klimesch. In turn our findings on upper frequency α oscillations are more often related to feature specific processes (see e.g. Figure 7), which could be related to the findings on upper frequency α by Klimesch. He related upper frequency α power to memory performance under high cognitive load, which in turn could be a proxy for how well the stimuli (i.e. its features) were encoded. A second publication by Rodriguez-Larios et al. (2022) [19] employed a single-subject analysis of independent components which revealed two dissociable α rhythms, which both were differentially modulated by visual distractors. The lower α component increased in power, while the higher frequency α component decreased in power under the presence of a visual distractor. Behavioural accuracy was positively related with lower frequency α power and negatively related with upper frequency α. Again, we interpret those findings as indirect evidence to support the here presented results, with the lower frequency α being related to attentional processes (i.e. distractor suppression) and the

upper frequency α to the content of the memory. Furthermore, it could be shown that individual α frequency (IAF) and task performance are related such that higher IAF is linked to higher visual task accuracy [102–104]. Coldea and colleagues (2022) [104] argue that the IAF modulates the speed of visual sampling, which is in line with Di Gregorio et al. (2022) [102]. Since behavioral performance in the present study was consistently high at 94% on average and subjects were asked to respond to a potential oddball as quickly as possible, a higher α frequency might reflect a more successful stimulus encoding and hence faster and more accuracte behavioral performance.

In addition α amplitude and frequency have been shown to reflect two distinct processes, where α frequency is related to task performance, amplitude could be demonstrated to be related to visual awareness or confidence judgements about individual task performance [103, 105, 106] that could even be shown to depend on the exact cortical region [107]. Taken together, the here observed upwards shift in frequency for the feature specific BOLD with sign flip (see Figure 7) is in line with those findings and most likely reflects a process different from general modulatory processes that are more reflected by broadband or low frequency α.

Not only did we find a dissociation in the frequency domain between the relationship of α and the BOLD signal, but furthermore found that the laminar activation patterns provide further insight into multiple α-related processes. Low frequency α is related predominantly to the BOLD signal in superficial layers (except feature specific BOLD increase voxels with incongruent EEG feature pairing where the SNR is limited due to the focus on positive signal changes only), while the higher frequency α could be associated predominantly to superficial *and* deep layer activity. Superficial layer activity has been shown to be under modulation of attention [18, 83, 94, 108], but mostly feedback related cortical activity in deep layers has been associated with stimulus features [26] and (feature) predictions [108]. As brought forward by Bastos et al. (2020) [108] in the context of stimulus predictability, α band activity in deep layers might be more related the predictability of certain stimulus features and superficial α being more generally modulated (irrespective of stimulus features). This would further be in line with findings by Pluta et al. (2019) [109], who could demonstrate in mice, that superficial layer activity acts suppressive on deep layers in order to fine tune stimulus feature selectivity.

One remaining question would be, whether already prestimulus α band activity in the upper range is predictive for task performance, as suggested by some authors [102, 103] and whether the laminar profile would be similar to the here presented findings on post-stimulus α. Due to the limited time window prior to the stimulus onset and gradient artifacts of the MRI machine that lasted until 300 ms before the onset of the stimulus, pre-stiumulus α could not be investigated in depth here. Figure 2 B however, indicates that pre-stimulus α might play a role for the present task.

A second remaining question is the relationship between the observed α and γ band effects. For the congruence contrast of feature specific voxels the strongest effects have been observed in superficial layers, followed by deep layers, which again supports the hypothesis that this deep layer effect is at least partly related to feature related processing. If and how lower and upper-frequency α band oscillations across different cortical layers interact with each other and how each or both interact with γ band oscillations [8], needs to be investigated in detail in future experiments.

Future publications will furthermore need to take β band oscillations into account as well, as those are hypothesized to play a crucial role for visual stimulus processing and might exert a potential top-down influence [7, 110]. Here, we only looked at β band oscillations exploratory and found no significant correlation between β and the BOLD signal. This could be due to the selection process for the respective EEG virtual channels that were optimized specifically for α, but furthermore could be explained by the burst-like nature of β oscillations [110, 111] which makes them harder to capture with the analysis strategies employed here.

Conclusion

In sum, we present evidence for the presence of multiple α - related processes in the visual system. While deep layer α appears to be related to the processing of specific stimulus features, superficial layer α appears related to a more general modulation of BOLD activity. In addition, the active stimulus feature processing appears tightly linked to γ band oscillations via superficial and deep layers as well.

Acknowledgments

The authors would like to thank Jan Mathijs Schoffelen, Simon Homölle and Robert Oostenveld for their support with EEG source modelling. Furthermore, we would like to thank Rüdiger Stirnberg for his support on setting up the interleaved fMRI sequence, as well as Tim van Mourik for his support on cortical layer segmentation and Laurentius Huber for providing the crucial hint on accurate fMRI sub-millimeter within and between block volume (co-) registration and motion parameter estimation. Furthermore, the authors would like to thank Koen Haak for fruitful discussions and vital support in setting up the pRF recording pipeline, as well as Matthias Ekman for fruitful discussions on the improvement of the pRF mapping analysis pipeline. Lastly, the authors would like to thank Ole Jensen, Floris de Lange, David Norris and Jérémie Mattout for fruitful discussions and Paul Gaalman and the DCCN technical group for outstanding support.

Funding

This work was supported by the European Research Council under the European Union's Seventh Framework Programme (FP7/2007–2013)/ERC starting grant (grant number 716862) attributed to Mathilde Bonnefond and the Fondation pour la Recherche Medicale - grant ID FDT202106013010 awarded to Tommy Clausner. This work was conducted in the framework of the LabEx Cortex ("Construction, Function and Cognitive Function and Rehabilitation of the Cortex," ANR-10-LABX-0042) of Université de Lyon.

References

[1] Dora Hermes, Natalia Petridou, Kendrick N Kay, and Jonathan Winawer. An image-computable model for

the stimulus selectivity of gamma oscillations. *Elife*, 8:e47035, 2019.

[2] Vinay Shirhatti, Poojya Ravishankar, and Supratim Ray. Gamma oscillations in primate primary visual cortex are severely attenuated by small stimulus discontinuities. *PLoS biology*, 20(6):e3001666, 2022.

[3] Jarrod Robert Dowdall, Marius Schneider, and Martin Vinck. Attentional modulation of inter-areal coherence explained by frequency shifts. *NeuroImage*, 277: 120256, 2023.

[4] Marius Schneider, Ana Clara Broggini, Benjamin Dann, Athanasia Tzanou, Cem Uran, Swathi Sheshadri, Hansjörg Scherberger, and Martin Vinck. A mechanism for inter-areal coherence through communication based on connectivity and oscillatory power. *Neuron*, 109(24):4050–4067.e12, December 2021. ISSN 08966273. doi: 10.1016/j.neuron.2021.09.037. URL https://linkinghub.elsevier.com/retrieve/pii/S0896627321007108.

[5] Pascal Fries. Neuronal gamma-band synchronization as a fundamental process in cortical computation. *Annual review of neuroscience*, 32:209–224, 2009.

[6] Pascal Fries. Rhythms for Cognition: Communication through Coherence. *Neuron*, 88(1):220–235, October 2015. ISSN 08966273. doi: 10.1016/j.neuron.2015.09.034. URL https://linkinghub.elsevier.com/retrieve/pii/S0896627315008235.

[7] Andre M Bastos, W Martin Usrey, Rick A Adams, George R Mangun, Pascal Fries, and Karl J Friston. Canonical microcircuits for predictive coding. *Neuron*, 76(4):695–711, 2012.

[8] Mathilde Bonnefond, Sabine Kastner, and Ole Jensen. Communication between Brain Areas Based on Nested Oscillations. *eneuro*, 4(2):ENEURO.0153–16.2017, 2017. ISSN 2373-2822. doi: 10.1523/ENEURO.0153-16.2017. URL http://eneuro.sfn.org/lookup/doi/10.1523/ENEURO.0153-16.2017.

[9] Wolfgang Klimesch, Paul Sauseng, and Simon Hanslmayr. EEG alpha oscillations: The inhibition–timing hypothesis. *Brain Research Reviews*, 53(1):63–88, January 2007. ISSN 01650173. doi: 10.1016/j.brainresrev.2006.06.003. URL http://linkinghub.elsevier.com/retrieve/pii/S016501730600083X.

[10] Gert Pfurtscheller, A Stancak Jr, and Ch Neuper. Event-related synchronization (ers) in the alpha band—an electrophysiological correlate of cortical idling: a review. *International journal of psychophysiology*, 24(1-2):39–46, 1996.

[11] Jianrong Jia, Ying Fan, and Huan Luo. Alpha-band phase modulates bottom-up feature processing. *Cerebral Cortex*, 32(6):1260–1268, 2022.

[12] Kun Song, Ming Meng, Lin Chen, Ke Zhou, and Huan Luo. Behavioral oscillations in attention: rhythmic α pulses mediated through θ band. *Journal of Neuroscience*, 34(14):4837–4844, 2014.

[13] Andreas Wutz, David Melcher, and Jason Samaha. Frequency modulation of neural oscillations according to visual task demands. *Proceedings of the National Academy of Sciences*, 115(6):1346–1351, 2018.

[14] Satu Palva and J. Matias Palva. New vistas for α-frequency band oscillations. *Trends in Neurosciences*, 30(4):150–158, April 2007. ISSN 01662236. doi: 10.1016/j.tins.2007.02.001. URL https://linkinghub.elsevier.com/retrieve/pii/S0166223607000264.

[15] Mathilde Bonnefond, Ole Jensen, and Tommy Clausner. Visual processing by hierarchical and dynamic multiplexing supported by phase coding. *PsyArXiv. November*, 24, 2023.

[16] Timo van Kerkoerle, Matthew W. Self, Bruno Dagnino, Marie-Alice Gariel-Mathis, Jasper Poort, Chris van der Togt, and Pieter R. Roelfsema. Alpha and Gamma Oscillations Characterize Feedback and Feedforward Processing in Monkey Visual Cortex. *Proceedings of the National Academy of Sciences*, 111(40):14332–14341, October 2014. ISSN 0027-8424, 1091-6490. doi: 10.1073/pnas.1402773111.

[17] S. Haegens, A. Barczak, G. Musacchia, M. L. Lipton, A. D. Mehta, P. Lakatos, and C. E. Schroeder. Laminar Profile and Physiology of the Rhythm in Primary Visual, Auditory, and Somatosensory Regions of Neocortex. *Journal of Neuroscience*, 35(42):14341–14352, October 2015. ISSN 0270-6474, 1529-2401. doi: 10.1523/JNEUROSCI.0600-15.2015. URL http://www.jneurosci.org/cgi/doi/10.1523/JNEUROSCI.0600-15.2015.

[18] René Scheeringa, Peter J. Koopmans, Tim van Mourik, Ole Jensen, and David G. Norris. The relationship between oscillatory EEG activity and the laminar-specific BOLD signal. *Proceedings of the National Academy of Sciences*, 113(24):6761–6766, June 2016. ISSN 0027-8424, 1091-6490. doi: 10.1073/pnas.1522577113. URL http://www.pnas.org/lookup/doi/10.1073/pnas.1522577113.

[19] Julio Rodriguez-Larios, Alma ElShafei, Melanie Wiehe, and Saskia Haegens. Visual working memory recruits two functionally distinct alpha rhythms in posterior cortex. *bioRxiv*, pages 2022–04, 2022.

[20] Y. B. Saalmann, M. A. Pinsk, L. Wang, X. Li, and S. Kastner. The Pulvinar Regulates Information Transmission Between Cortical Areas Based on Attention Demands. *Science*, 337(6095):753–756, August 2012. ISSN 0036-8075, 1095-9203. doi: 10.1126/science.1223082. URL http://www.sciencemag.org/cgi/doi/10.1126/science.1223082.

[21] Diego Lozano-Soldevilla and Rufin VanRullen. The hidden spatial dimension of alpha: 10-hz perceptual echoes propagate as periodic traveling waves in the human brain. *Cell reports*, 26(2):374–380, 2019.

[22] Ben M Harvey, Mariska J Vansteensel, Cyrille H Ferrier, Natalia Petridou, Wietske Zuiderbaan, Erik J Aarnoutse, Martin G Bleichner, H Chris Dijkerman, Martine JE van Zandvoort, Frans SS Leijten, et al. Frequency specific spatial interactions in human electrocorticography: V1 alpha oscillations reflect surround suppression. *Neuroimage*, 65:424–432, 2013.

[23] Supratim Ray and John HR Maunsell. Do gamma oscillations play a role in cerebral cortex? *Trends in cognitive sciences*, 19(2):78–85, 2015.

[24] René Scheeringa, Mathilde Bonnefond, Tim van Mourik, Ole Jensen, David G Norris, and Peter J Koopmans. Relating neural oscillations to laminar fmri connectivity in visual cortex. *Cerebral Cortex*, 2022.

[25] James J Bonaiuto, Simon Little, Samuel A Neymotin, Stephanie R Jones, Gareth R Barnes, and Sven Bestmann. Laminar dynamics of high amplitude beta bursts in human motor cortex. *Neuroimage*, 242: 118479, 2021.

[26] Peter Kok, Lauren J. Bains, Tim van Mourik, David G. Norris, and Floris P. de Lange. Selective Activation of the Deep Layers of the Human Primary Visual Cortex by Top-Down Feedback. *Current Biology*, 26(3):371–376, February 2016. ISSN 09609822. doi: 10.1016/j.cub.2015.12.038. URL http://linkinghub.elsevier.com/retrieve/pii/S0960982215015699.

[27] Samuel J.D. Lawrence, Elia Formisano, Lars Muckli, and Floris P. de Lange. Laminar fMRI: Applications for cognitive neuroscience. *NeuroImage*, July 2017. ISSN 10538119. doi: 10.1016/j.neuroimage.2017.07.004. URL http://linkinghub.elsevier.com/retrieve/pii/S1053811917305724.

[28] Matthew W. Self, Timo van Kerkoerle, Rainer Goebel, and Pieter R. Roelfsema. Benchmarking laminar fMRI: Neuronal spiking and synaptic activity during top-down and bottom-up processing in the different layers of cortex. *NeuroImage*, 197:806–817, August 2019. ISSN 10538119. doi: 10.1016/j.neuroimage.2017.06.045. URL https://linkinghub.elsevier.com/retrieve/pii/S1053811917305177.

[29] K.E. Stephan, F.H. Petzschner, L. Kasper, J. Bayer, K.V. Wellstein, G. Stefanics, K.P. Pruessmann, and J. Heinzle. Laminar fMRI and computational theories of brain function. *NeuroImage*, 197:699–706, August 2019. ISSN 10538119. doi: 10.1016/j.neuroimage.2017.11.001. URL https://linkinghub.elsevier.com/retrieve/pii/S1053811917309084.

[30] Jiajia Yang, Laurentius Huber, Yinghua Yu, and Peter A. Bandettini. Linking cortical circuit models to human cognition with laminar fMRI. *Neuroscience & Biobehavioral Reviews*, 128:467–478, September 2021. ISSN 01497634. doi: 10.1016/j.neubiorev.2021.07.005. URL https://linkinghub.elsevier.com/retrieve/pii/S0149763421003031.

[31] René Scheeringa and Pascal Fries. Cortical layers, rhythms and bold signals. *NeuroImage*, 197:689–698, 2019.

[32] Rukun Hinz, Lore M Peeters, Disha Shah, Stephan Missault, Michaël Belloy, Verdi Vanreusel, Meriam Malekzadeh, Marleen Verhoye, Annemie Van der Linden, and Georgios A Keliris. Bottom-up sensory processing can induce negative bold responses and reduce functional connectivity in nodes of the default mode-like network in rats. *Neuroimage*, 197:167–176, 2019.

[33] Stephen D Mayhew, Dirk Ostwald, Camillo Porcaro, and Andrew P Bagshaw. Spontaneous eeg alpha oscillation interacts with positive and negative bold responses in the visual–auditory cortices and default-mode network. *Neuroimage*, 76:362–372, 2013.

[34] Marcus E Raichle, Ann Mary MacLeod, Abraham Z Snyder, William J Powers, Debra A Gusnard, and Gordon L Shulman. A default mode of brain function. *Proceedings of the national academy of sciences*, 98 (2):676–682, 2001.

[35] Roger BH Tootell, Nouchine Hadjikhani, E Kevin Hall, Sean Marrett, Wim Vanduffel, J Thomas Vaughan, and Anders M Dale. The retinotopy of visual spatial attention. *Neuron*, 21(6):1409–1422, 1998.

[36] Amir Shmuel, Mark Augath, Axel Oeltermann, and Nikos K Logothetis. Negative functional mri response correlates with decreases in neuronal activity in monkey visual area v1. *Nature neuroscience*, 9(4):569–577, 2006.

[37] Timo Van Kerkoerle, Matthew W Self, and Pieter R Roelfsema. Layer-specificity in the effects of attention and working memory on activity in primary visual cortex. *Nature communications*, 8(1):1–14, 2017.

[38] M Brant-Zawadzki, G D Gillan, and W R Nitz. MP RAGE: a three-dimensional, T1-weighted, gradient-echo sequence–initial experience in the brain. *Radiology*, 182(3):769–775, March 1992. ISSN 0033-8419, 1527-1315. doi: 10.1148/radiology.182.3.1535892. URL http://pubs.rsna.org/doi/10.1148/radiology.182.3.1535892.

[39] B.A. Poser, P.J. Koopmans, T. Witzel, L.L. Wald, and M. Barth. Three dimensional echo-planar imaging at 7 Tesla. *NeuroImage*, 51(1):261–266, May 2010. ISSN 10538119. doi: 10.1016/j.neuroimage.2010.01.108. URL http://linkinghub.elsevier.com/retrieve/pii/S1053811910001473.

[40] Mayur Narsude, Daniel Gallichan, Wietske Van Der Zwaag, Rolf Gruetter, and José P Marques. Three-dimensional echo planar imaging with controlled aliasing: a sequence for high temporal resolution functional mri. *Magnetic resonance in medicine*, 75(6): 2350–2361, 2016.

[41] Rüdiger Stirnberg, Willem Huijbers, Daniel Brenner, Benedikt A Poser, Monique Breteler, and Tony Stöcker. Rapid whole-brain resting-state fmri at 3 t: Efficiency-optimized three-dimensional epi versus repetition time-matched simultaneous-multi-slice epi. *Neuroimage*, 163:81–92, 2017.

[42] Brain Products Inc, GmbH, Munich, Germany. Brain Products, 2018.

[43] Tommy Clausner, Sarang S. Dalal, and Maité Crespo-García. Photogrammetry-Based Head Digitization for Rapid and Accurate Localization of EEG Electrodes and MEG Fiducial Markers Using a Single Digital SLR Camera. *Frontiers in Neuroscience*, 11, May 2017. ISSN 1662-453X. doi: 10.3389/fnins.2017.00264.

[44] SR Research. EyeLink 1000 Plus - The Most Flexible Eye Tracker. *SR Research*, 2018.

[45] Tim Van Mourik, Jan PJM van der Eerden, Pierre-Louis Bazin, and David G Norris. Laminar signal extraction over extended cortical areas by means of a spatial glm. *PloS one*, 14(3):e0212493, 2019.

[46] Neurobehavioral Systems, Inc. Neurobehavioral Systems, 2018.

[47] L. Thaler, A.C. Schütz, M.A. Goodale, and K.R. Gegenfurtner. What Is the Best Fixation Target? The Effect of Target Shape on Stability of Fixational Eye Movements. *Vision Research*, 76:31–42, January 2013. ISSN 00426989. doi: 10.1016/j.visres.2012.10.012.

[48] M. J. Arcaro, S. A. McMains, B. D. Singer, and S. Kastner. Retinotopic Organization of Human Ventral Visual Cortex. *Journal of Neuroscience*, 29(34): 10638–10652, August 2009. ISSN 0270-6474, 1529-2401. doi: 10.1523/JNEUROSCI.2807-09.2009.

[49] Brian A Wandell, Suelika Chial, and Benjamin T Backus. Visualization and measurement of the cortical surface. *Journal of cognitive neuroscience*, 12(5): 739–752, 2000.

[50] David H. Brainard. The Psychophysics Toolbox. *Spatial Vision*, 10:433–436, 1997.

[51] Ivan Alvarez, De Haas, Benjamin A, Chris A. Clark, Geraint Rees, and D. Samuel Schwarzkopf. Comparing different stimulus configurations for population receptive field mapping in human fMRI. *Frontiers in Human Neuroscience*, 9, 2015. ISSN 1662-5161. doi: 10.3389/fnhum.2015.00096. URL https://www.frontiersin.org/articles/10.3389/fnhum.2015.00096/full.

[52] Ho-Ling Liu and Jia-Hong Gao. An investigation of the impulse functions for the nonlinear BOLD response in functional MRI. *Magnetic Resonance Imaging*, 18(8): 931–938, October 2000. ISSN 0730725X. doi: 10.1016/S0730-725X(00)00214-9. URL http://linkinghub.elsevier.com/retrieve/pii/S0730725X00002149.

[53] Serge O. Dumoulin and Brian A. Wandell. Population receptive field estimates in human visual cortex. *NeuroImage*, 39(2):647–660, January 2008. ISSN 10538119. doi: 10.1016/j.neuroimage.2007.09.034. URL http://linkinghub.elsevier.com/retrieve/pii/S1053811907008269.

[54] Kendrick N. Kay, Jonathan Winawer, Aviv Mezer, and Brian A. Wandell. Compressive Spatial Summation in Human Visual Cortex. *Journal of Neurophysiology*, 110(2):481–494, July 2013. ISSN 0022-3077, 1522-1598. doi: 10.1152/jn.00105.2013.

[55] Brian B. Avants, Nicholas J. Tustison, Gang Song, Philip A. Cook, Arno Klein, and James C. Gee. A reproducible evaluation of ANTs similarity metric performance in brain image registration. *NeuroImage*, 54(3):2033–2044, February 2011. ISSN 10538119. doi: 10.1016/j.neuroimage.2010.09.025. URL https://linkinghub.elsevier.com/retrieve/pii/S1053811910012061.

[56] Robert Oostenveld, Pascal Fries, Eric Maris, and Jan-Mathijs Schoffelen. FieldTrip: Open Source Software for Advanced Analysis of MEG, EEG, and Invasive Electrophysiological Data. *Computational Intelligence and Neuroscience*, 2011:1–9, 2011. ISSN 1687-5265, 1687-5273. doi: 10.1155/2011/156869.

[57] Bruce Fischl. FreeSurfer. *NeuroImage*, 62(2):774–781, August 2012. ISSN 10538119. doi: 10.1016/j.neuroimage.2012.01.021.

[58] Stephen M. Smith, Mark Jenkinson, Mark W. Woolrich, Christian F. Beckmann, Timothy E.J. Behrens, Heidi Johansen-Berg, Peter R. Bannister, Marilena De Luca, Ivana Drobnjak, David E. Flitney, Rami K. Niazy, James Saunders, John Vickers, Yongyue Zhang, Nicola De Stefano, J. Michael Brady, and Paul M. Matthews. Advances in Functional and Structural MR Image Analysis and Implementation as FSL. *NeuroImage*, 23:S208–S219, January 2004. ISSN 10538119. doi: 10.1016/j.neuroimage.2004.07.051.

[59] Agisoft, St Petersburg, Russia, LLC. Agisoft Metashape. *Educational Edition*, 2014. URL https://www.agisoft.com/buy/online-store/educational-license/.

[60] C Rorden, HO Karnath, and L Bonilha. MRIcron Dicom to Nifti Converter. *Neuroimaging Informatics Tools and Resources Clearinghouse (NITRC)*, 2012.

[61] Tommy Clausner. MRI Volume Masker 3000 TM, October 2022. URL https://doi.org/10.5281/zenodo.7211757.

[62] K. J. Friston, editor. *Statistical parametric mapping: the analysis of functional brain images*. Elsevier/Academic Press, Amsterdam ; Boston, 1st ed edition, 2007. ISBN 978-0-12-372560-8.

[63] Washington-University. Workbench, 2018. URL https://github.com/Washington-University/workbench.

[64] B Avants, C Epstein, M Grossman, and J Gee. Symmetric diffeomorphic image registration with cross-correlation: Evaluating automated labeling of elderly and neurodegenerative brain. *Medical Image Analysis*, 12(1):26–41, February 2008. ISSN 13618415. doi: 10.1016/j.media.2007.06.004. URL https://linkinghub.elsevier.com/retrieve/pii/S1361841507000606.

[65] Oscar Esteban, Christopher J. Markiewicz, Ross W. Blair, Craig A. Moodie, A. Ilkay Isik, Asier Erramuzpe, James D. Kent, Mathias Goncalves, Elizabeth DuPre, Madeleine Snyder, Hiroyuki Oya, Satrajit S. Ghosh, Jessey Wright, Joke Durnez, Russell A. Poldrack, and Krzysztof J. Gorgolewski. fMRIPrep: a robust preprocessing pipeline for functional MRI. *Nature Methods*, 16(1):111–116, January 2019. ISSN 1548-7091, 1548-7105. doi: 10.1038/s41592-018-0235-4. URL http://www.nature.com/articles/s41592-018-0235-4.

[66] Liang Wang, Ryan E.B. Mruczek, Michael J. Arcaro, and Sabine Kastner. Probabilistic Maps of Visual Topography in Human Cortex. *Cerebral Cortex*, 25(10):3911–3931, October 2015. ISSN

1047-3211, 1460-2199. doi: 10.1093/cercor/bhu277. URL https://academic.oup.com/cercor/article-lookup/doi/10.1093/cercor/bhu277.

[67] Rebecca Shafee, Randy L. Buckner, and Bruce Fischl. Gray matter myelination of 1555 human brains using partial volume corrected MRI images. *NeuroImage*, 105:473–485, January 2015. ISSN 10538119. doi: 10.1016/j.neuroimage.2014.10.054. URL http://linkinghub.elsevier.com/retrieve/pii/S1053811914008933.

[68] Tim Van Mourik, Jan PJM van der Eerden, Pierre-Louis Bazin, and David G Norris. Laminar signal extraction over extended cortical areas by means of a spatial glm. *PloS one*, 14(3):e0212493, 2019.

[69] Barry D. Van Veen and Kevin M. Buckley. Beamforming: A Versatile Approach to Spatial Filtering. *IEEE assp magazine*, 5(2):4–24, 1988. URL http://users.isy.liu.se/en/rt/fredrik/spcourse/beamform.pdf.

[70] P. Adjamian, S.F. Worthen, A. Hillebrand, P.L. Furlong, B.A. Chizh, A.R. Hobson, Q. Aziz, and G.R. Barnes. Effective electromagnetic noise cancellation with beamformers and synthetic gradiometry in shielded and partly shielded environments. *Journal of Neuroscience Methods*, 178(1):120–127, March 2009. ISSN 01650270. doi: 10.1016/j.jneumeth.2008.12.006. URL http://linkinghub.elsevier.com/retrieve/pii/S0165027008006808.

[71] Matthew J. Brookes, Karen J. Mullinger, Claire M. Stevenson, Peter G. Morris, and Richard Bowtell. Simultaneous EEG source localisation and artifact rejection during concurrent fMRI by means of spatial filtering. *NeuroImage*, 40(3):1090–1104, April 2008. ISSN 10538119. doi: 10.1016/j.neuroimage.2007.12.030. URL http://linkinghub.elsevier.com/retrieve/pii/S1053811907011500.

[72] Matthew J. Brookes, Jiri Vrba, Karen J. Mullinger, Gerða Björk Geirsdóttir, Winston X. Yan, Claire M. Stevenson, Richard Bowtell, and Peter G. Morris. Source localisation in concurrent EEG/fMRI: Applications at 7T. *NeuroImage*, 45(2):440–452, April 2009. ISSN 10538119. doi: 10.1016/j.neuroimage.2008.10.047. URL http://linkinghub.elsevier.com/retrieve/pii/S1053811908011609.

[73] Johannes Vorwerk, Robert Oostenveld, Maria Carla Piastra, Lilla Magyari, and Carsten H. Wolters. The FieldTrip-SimBio pipeline for EEG forward solutions. *BioMedical Engineering OnLine*, 17(1), December 2018. ISSN 1475-925X. doi: 10.1186/s12938-018-0463-y. URL https://biomedical-engineering-online.biomedcentral.com/articles/10.1186/s12938-018-0463-y.

[74] S. Baillet, J. C. Mosher, and R. M. Leahy. Electromagnetic brain mapping. *IEEE Signal Processing Magazine*, 18(6):14–30, November 2001. ISSN 1053-5888. doi: 10.1109/79.962275.

[75] Christoph M Michel, Gregor Thut, Stéphanie Morand, Asaid Khateb, Alan J Pegna, Rolando Grave de Peralta, Sara Gonzalez, Margitta Seeck, and Theodor Landis. Electric source imaging of human brain functions. *Brain Research Reviews*, 36(2):108–118, October 2001. ISSN 0165-0173. doi: 10.1016/S0165-0173(01)00086-8. URL http://www.sciencedirect.com/science/article/pii/S0165017301000868.

[76] D. Slepian. Prolate Spheroidal Wave Functions, Fourier Analysis, and Uncertainty-V: The Discrete Case. *Bell System Technical Journal*, 57(5):1371–1430, May 1978. ISSN 00058580. doi: 10.1002/j.1538-7305.1978.tb02104.x. URL https://ieeexplore.ieee.org/document/6771595.

[77] Rosanne M Van Diepen, John J Foxe, and Ali Mazaheri. The functional role of alpha-band activity in attentional processing: the current zeitgeist and future outlook. *Current opinion in psychology*, 29:229–238, 2019.

[78] Joachim Gross, Jan Kujala, Matti Hämäläinen, Lars Timmermann, Alfons Schnitzler, and Riitta Salmelin. Dynamic imaging of coherent sources: studying neural interactions in the human brain. *Proceedings of the National Academy of Sciences*, 98(2):694–699, 2001.

[79] MathWorks. MATLAB, 2021. URL https://www.mathworks.com/store/.

[80] Eric Maris and Robert Oostenveld. Nonparametric statistical testing of EEG- and MEG-data. *Journal of Neuroscience Methods*, 164(1):177–190, August 2007. ISSN 0165-0270. doi: 10.1016/j.jneumeth.2007.03.024. URL https://www.sciencedirect.com/science/article/pii/S0165027007001707.

[81] Tommy Clausner and Stefano Gentili. Auto-regressive Rank Order Similarity (aros) test, June 2022. URL https://www.biorxiv.org/content/10.1101/2022.06.15.496113v1. Pages: 2022.06.15.496113 Section: New Results.

[82] Samuel J. D. Lawrence, Tim van Mourik, Peter Kok, Peter J. Koopmans, David G. Norris, and Floris P. de Lange. Laminar Organization of Working Memory Signals in Human Visual Cortex. *Current Biology*, 28(21):3435–3440.e4, November 2018. ISSN 0960-9822. doi: 10.1016/j.cub.2018.08.043. URL https://www.cell.com/current-biology/abstract/S0960-9822(18)31127-8. Publisher: Elsevier.

[83] Samuel JD Lawrence, David G Norris, and Floris P de Lange. Dissociable laminar profiles of concurrent bottom-up and top-down modulation in the human visual cortex. *eLife*, 8:e44422, May 2019. ISSN 2050-084X. doi: 10.7554/eLife.44422. URL https://doi.org/10.7554/eLife.44422. Publisher: eLife Sciences Publications, Ltd.

[84] Irati Markuerkiaga, José P Marques, Lauren J Bains, and David G Norris. An in-vivo study of bold laminar responses as a function of echo time and static magnetic field strength. *Scientific reports*, 11(1):1–13, 2021.

[85] Johanna M Zumer, René Scheeringa, Jan-Mathijs Schoffelen, David G Norris, and Ole Jensen. Occipital

alpha activity during stimulus processing gates the information flow to object-selective cortex. *PLoS biology*, 12(10):e1001965, 2014.

[86] Teresa Murta, Marco Leite, David W Carmichael, Patrícia Figueiredo, and Louis Lemieux. Electrophysiological correlates of the bold signal for eeg-informed fmri. *Human brain mapping*, 36(1):391–414, 2015.

[87] Yoav Benjamini and Yosef Hochberg. Controlling the false discovery rate: a practical and powerful approach to multiple testing. *Journal of the Royal statistical society: series B (Methodological)*, 57(1):289–300, 1995.

[88] Dardo Tomasi, Thomas Ernst, Elisabeth C Caparelli, and Linda Chang. Common deactivation patterns during working memory and visual attention tasks: An intra-subject fmri study at 4 tesla. *Human brain mapping*, 27(8):694–705, 2006.

[89] Sofia Crespi, Laura Biagi, Giovanni d'Avossa, David C Burr, Michela Tosetti, and Maria Concetta Morrone. Spatiotopic coding of bold signal in human visual cortex depends on spatial attention. *PloS one*, 6(7): e21661, 2011.

[90] Sergio Chieffi, Clara Castaldi, Girolamo Di Maio, Marco La Marra, Antonietta Messina, Vincenzo Monda, and Ines Villano. Attentional bias in the radial and vertical dimensions of space. *Comptes rendus biologies*, 342(3-4):97–100, 2019.

[91] Maxwell Drain and Patricia A Reuter-Lorenz. Vertical orienting control: evidence for attentional bias and" neglect" in the intact brain. *Journal of Experimental Psychology: General*, 125(2):139, 1996.

[92] Stephen A Engel, Gary H Glover, and Brian A Wandell. Retinotopic organization in human visual cortex and the spatial precision of functional mri. *Cerebral cortex (New York, NY: 1991)*, 7(2):181–192, 1997.

[93] John-Dylan Haynes and Geraint Rees. Predicting the orientation of invisible stimuli from activity in human primary visual cortex. *Nature neuroscience*, 8(5):686–691, 2005.

[94] Mila Halgren, István Ulbert, Hélène Bastuji, Dániel Fabó, Lorand Erőss, Marc Rey, Orrin Devinsky, Werner K Doyle, Rachel Mak-McCully, Eric Halgren, et al. The generation and propagation of the human alpha rhythm. *Proceedings of the National Academy of Sciences*, 116(47):23772–23782, 2019.

[95] Floris P De Lange, Micha Heilbron, and Peter Kok. How do expectations shape perception? *Trends in cognitive sciences*, 22(9):764–779, 2018.

[96] Maryam Bijanzadeh, Lauri Nurminen, Sam Merlin, Andrew M Clark, and Alessandra Angelucci. Distinct laminar processing of local and global context in primate primary visual cortex. *Neuron*, 100(1):259–274, 2018.

[97] Marc Alwin Gieselmann and Alexander Thiele. Stimulus dependence of directed information exchange between cortical layers in macaque v1. *Elife*, 11: e62949, 2022.

[98] Demetrio Ferro, Jochem van Kempen, Michael Boyd, Stefano Panzeri, and Alexander Thiele. Directed information exchange between cortical layers in macaque v1 and v4 and its modulation by selective attention. *Proceedings of the National Academy of Sciences*, 118 (12):e2022097118, 2021.

[99] Nikola T. Markov, Julien Vezoli, Pascal Chameau, Arnaud Falchier, René Quilodran, Cyril Huissoud, Camille Lamy, Pierre Misery, Pascale Giroud, Shimon Ullman, Pascal Barone, Colette Dehay, Kenneth Knoblauch, and Henry Kennedy. Anatomy of hierarchy: Feedforward and feedback pathways in macaque visual cortex: Cortical counterstreams. *Journal of Comparative Neurology*, 522(1):225–259, January 2014. ISSN 00219967. doi: 10.1002/cne.23458. URL http://doi.wiley.com/10.1002/cne.23458.

[100] Ole Jensen and Ali Mazaheri. Shaping Functional Architecture by Oscillatory Alpha Activity: Gating by Inhibition. *Frontiers in Human Neuroscience*, 4, 2010. ISSN 1662-5161. doi: 10.3389/fnhum.2010.00186. URL http://journal.frontiersin.org/article/10.3389/fnhum.2010.00186/abstract.

[101] Wolfgang Klimesch. Eeg-alpha rhythms and memory processes. *International Journal of psychophysiology*, 26(1-3):319–340, 1997.

[102] Francesco Di Gregorio, Jelena Trajkovic, Cristina Roperti, Eleonora Marcantoni, Paolo Di Luzio, Alessio Avenanti, Gregor Thut, and Vincenzo Romei. Tuning alpha rhythms to shape conscious visual perception. *Current Biology*, 32(5):988–998, 2022.

[103] Jelena Trajkovic, Francesco Di Gregorio, Gregor Thut, and Vincenzo Romei. Transcranial magnetic stimulation effects support an oscillatory model of erp genesis. *Current Biology*, 2024.

[104] Andra Coldea, Domenica Veniero, Stephanie Morand, Jelena Trajkovic, Vincenzo Romei, Monika Harvey, and Gregor Thut. Effects of rhythmic transcranial magnetic stimulation in the alpha-band on visual perception depend on deviation from alpha-peak frequency: faster relative transcranial magnetic stimulation alpha-pace improves performance. *Frontiers in Neuroscience*, 16:886342, 2022.

[105] Christopher SY Benwell, Chiara F Tagliabue, Domenica Veniero, Roberto Cecere, Silvia Savazzi, and Gregor Thut. Prestimulus eeg power predicts conscious awareness but not objective visual performance. *eneuro*, 4(6), 2017.

[106] Christopher SY Benwell, Raquel E London, Chiara F Tagliabue, Domenica Veniero, Joachim Gross, Christian Keitel, and Gregor Thut. Frequency and power of human alpha oscillations drift systematically with time-on-task. *NeuroImage*, 192:101–114, 2019.

[107] Jason Samaha, Olivia Gosseries, and Bradley R Postle. Distinct oscillatory frequencies underlie excitability of human occipital and parietal cortex. *Journal of Neuroscience*, 37(11):2824–2833, 2017.

[108] André M Bastos, Mikael Lundqvist, Ayan S Waite, Nancy Kopell, and Earl K Miller. Layer and rhythm specificity for predictive routing. *Proceedings of the National Academy of Sciences*, 117(49):31459–31469, 2020.

[109] Scott R Pluta, Greg I Telian, Alexander Naka, and Hillel Adesnik. Superficial layers suppress the deep layers to fine-tune cortical coding. *Journal of Neuroscience*, 39(11):2052–2064, 2019.

[110] Viviana Betti, Stefania Della Penna, Francesco de Pasquale, and Maurizio Corbetta. Spontaneous beta band rhythms in the predictive coding of natural stimuli. *The Neuroscientist*, 27(2):184–201, 2021.

[111] James J Bonaiuto, Fardin Afdideh, Maxime Ferez, Konrad Wagstyl, Jérémie Mattout, Mathilde Bonnefond, Gareth R Barnes, and Sven Bestmann. Estimates of cortical column orientation improve meg source inversion. *Neuroimage*, 216:116862, 2020.

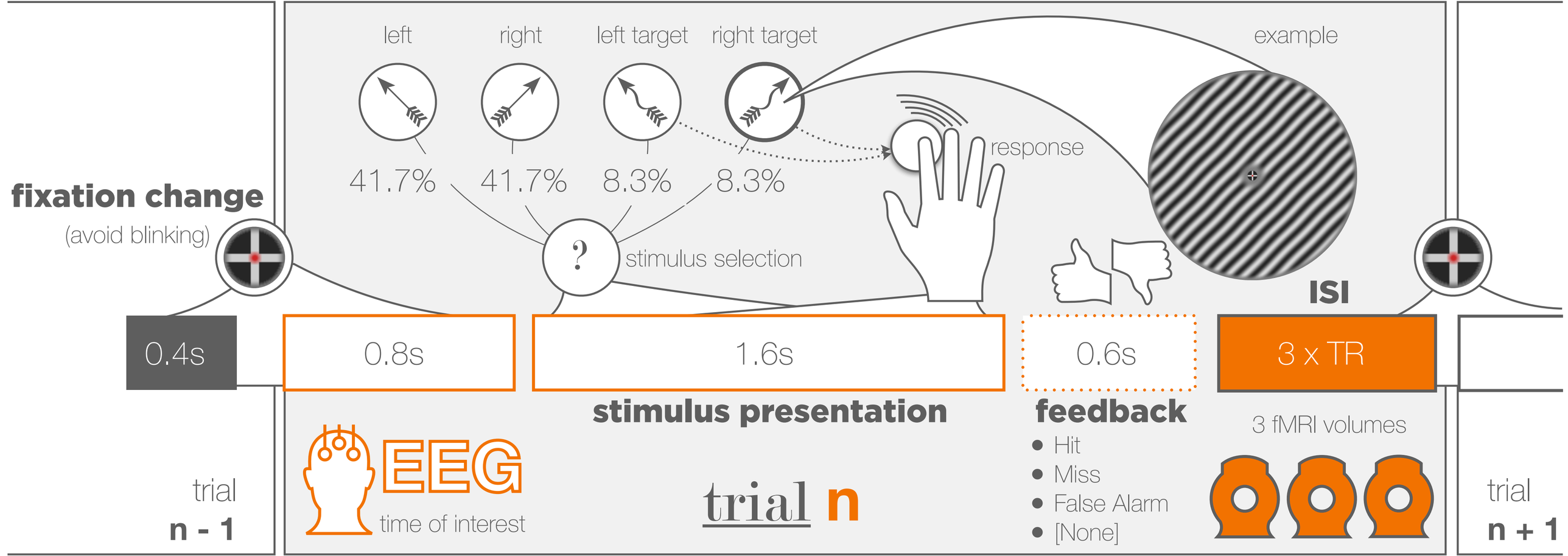
left
right
left target
right target
example
41.7%
41.7%
8.3%
8.3%
response
?
stimulus selection
fixation change
(avoid blinking)
ISI
0.4s
0.8s
1.6s
0.6s
3 x TR
stimulus presentation
feedback
Hit
Miss
False Alarm
[None]
3 fMRI volumes
EEG
time of interest
trial n
trial n - 1
trial n + 1

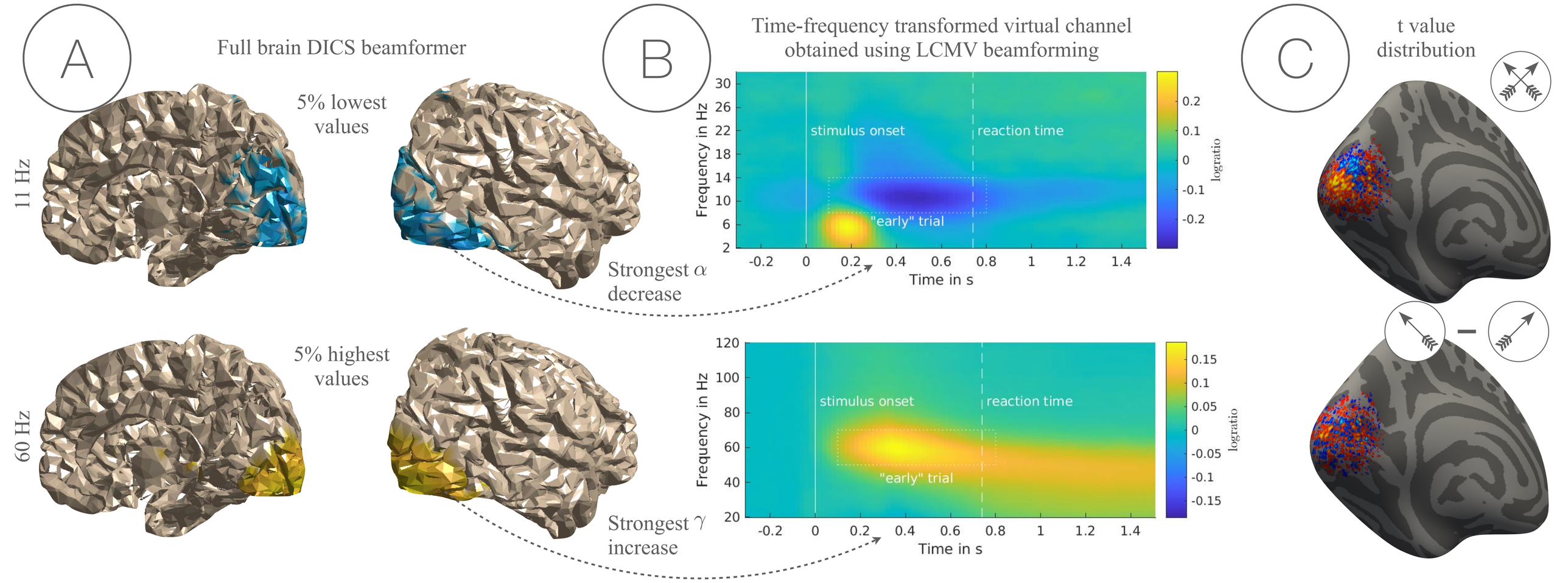
A
Full brain DICS beamformer
11 Hz
5% lowest values
60 Hz
5% highest values
B
Time-frequency transformed virtual channel obtained using LCMV beamforming
Frequency in Hz
Time in s
stimulus onset
reaction time
"early" trial
logratio
Strongest α decrease
Strongest γ increase
C
t value distribution

A

fMRI voxel

[CSF]

superficial

middle

deep

[white matter]

Cortical layer shells

CSF: 0.00

superficial layer: 0.00

middle layer: **0.12**

deep layer: **0.80**

white matter: **0.08**

Example:

B

Virtual EEG channels.
Optimised for **gamma** or **alpha**
Separately for each hemisphere

Time-Frequency analysis

2x

2x

100ms

400ms

gamma

400ms

alpha

Trial-by-trial power changes convolved with HRF are used as EEG-based fMRI regressors

One regressor **for each TF bin**.
Time bins from a sliding window (400ms length; shifted by 100ms)

C

Fixed fMRI task and nuisance regressors

Regression

EEG time and frequency specific regressor

fMRI first level contrasts and **voxel selection** based on t-values

l - r

R *L*

Orientation preference

r - BL *l - BL*

Positive response to preferred orientation

l - BL *r - BL*

Negative response to not preferred orientation

[Example]

Layer weights

$\beta_{voxel} \times \begin{bmatrix} w_{CSF} \\ w_{superficial} \\ w_{middle} \\ w_{deep} \\ w_{white} \end{bmatrix} = \begin{bmatrix} \beta_{CSF} \\ \beta_{superficial} \\ \beta_{middle} \\ \beta_{deep} \\ \beta_{white} \end{bmatrix}$

$\sum = 1 \qquad \sum = \beta_{voxel}$

average over:
- voxel
- exp. block
- time

D

Statistical inference on βs

Frequency

Subjects

Depth

Profile

aros test

cluster permutation test

Cortical layers

- superficial
- middle
- deep

Selection threshold

% most extreme t-values

Condition

congruent

incongruent - 25% - 10% - 5%

incongruent

α

EEG Frequency

$\bar{\beta}$ **coefficient**

γ

After MC correction

Significant Cluster test

Before MC correction

After MC correction

Significant rank order

Before MC correction

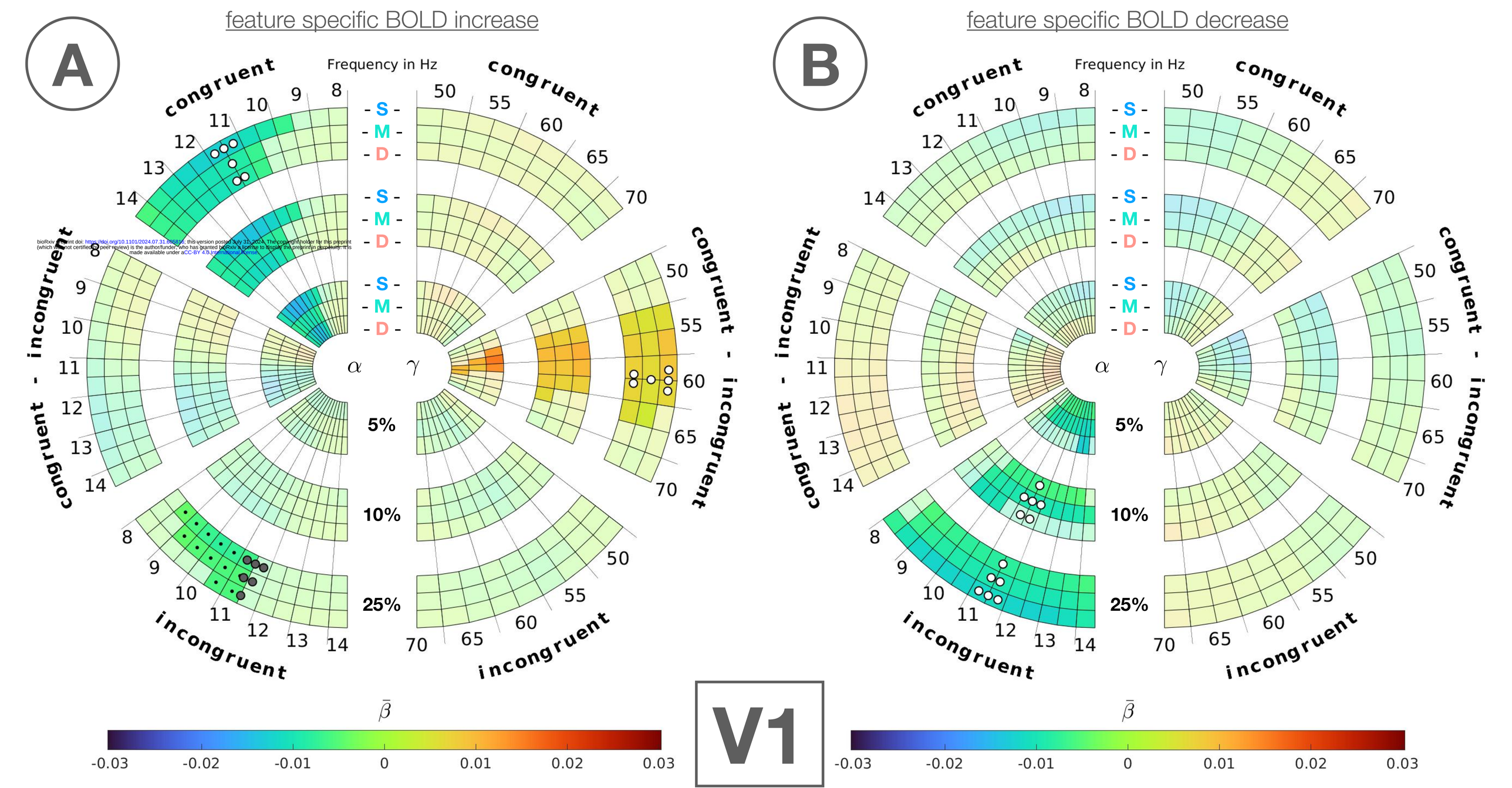

V1 feature specific BOLD sign flip

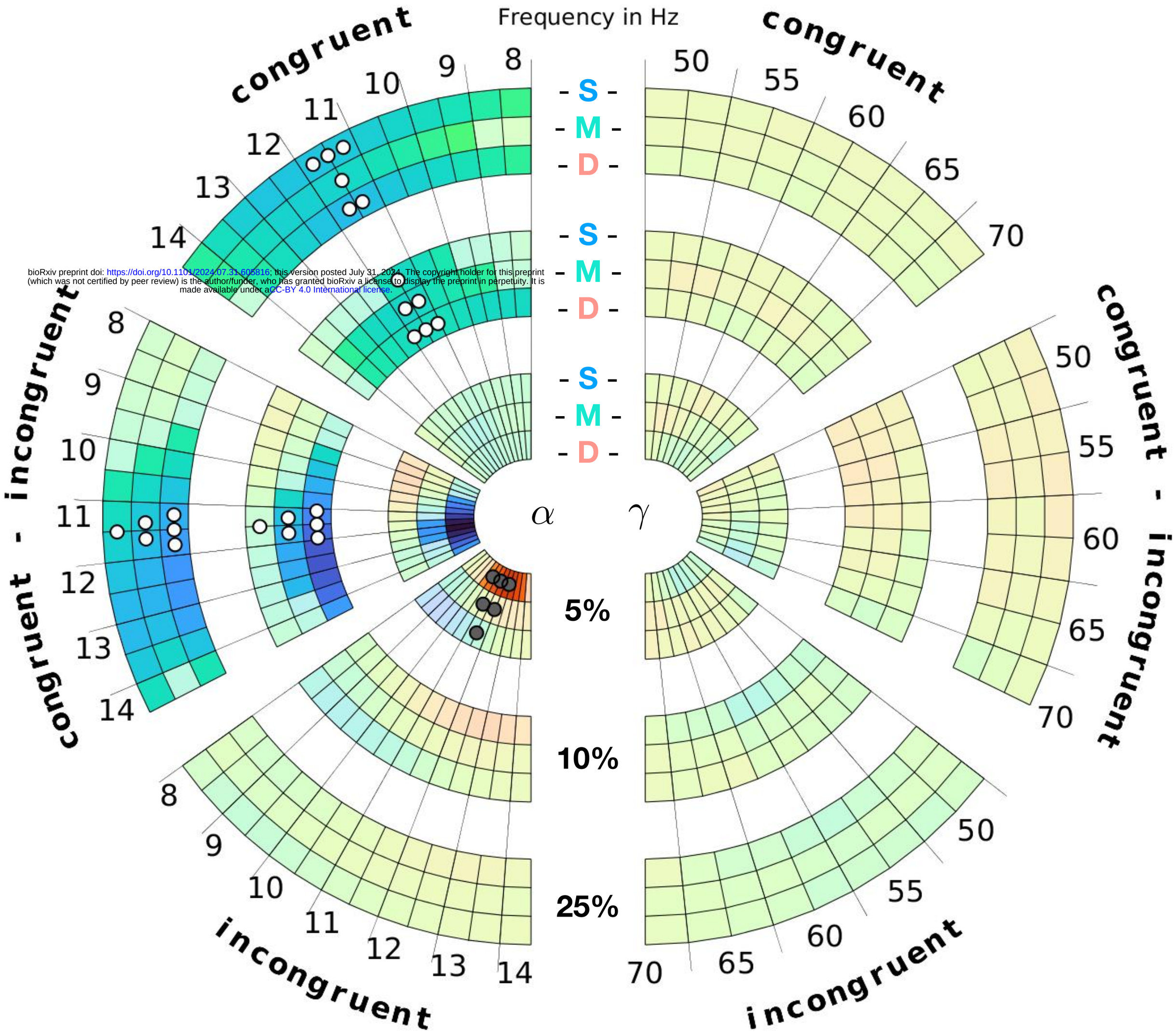

V1 feature unspecific BOLD decrease